Supporting Information

Table of Contents

General Information

Reagents and Methods. All X-ray structures described in this paper were obtained from https://www.rcsb.org/. All interaction interpretations were assisted by the LigPlot+ software,[SI1] and the molecular visualization with PyMOL.[SI2] Loop modeling and morphing simulation was computed using the loop modeling protocol DOPE-HR from the MODELLER add-on[SI3a] in the UCSF Chimera Software,[SI3b] and the resulting structure was completed in Interactive ROSETTA.[SI4] MD simulations to estimate the differences of motion between loops were tested using ToeLoop[SI5]. All reagents, Fmoc-amino acids and resins used in the present paper were purchased from Chemimpex and Millipore Sigma. All bulk solvents were acquired from Fischer Scientific. Assay kit for screening and profiling inhibitors of the PD-1/PD-L1 interaction was purchased from BPS Bioscience. Peptides, **1a-e, 2a-c** were synthesized using a standard automatized Fmoc-SPPS technique (solid-phase peptide synthesis) on a Protein Technologies PS-3 peptide synthesizer. Syntheses were accomplished on a Fmoc-Glu-Wang resin (0.4 meq/g). The peptides purity was measured by analytical reverse-phase high-performance liquid chromatography (RP-HPLC) on a Hitachi L-7000 series equipped with a XBridge BEH C_{18} column (130 Å, 10 µm, 4.6 mm x 250 mm) and their molecular weight determined by mass spectrometry using a Bruker Microflex LRF matrix-assisted laser desorption ionization time-of-flight (MALDI-TOF). Peptide solutions for circular dichroism (CD) were prepared at 20-100 µM concentration range in phosphate buffer (15 mM, pH 6.5) with addition of MeOH (up to 50% v/v) if required to increase solubility. Each sample concentration was determined accurately by measuring the solution UV-absorbance using a JASCO V-670 spectrophotometer based on the combined molar absorptivity of Trp (ε_{280} = 5580 $M^{-1}.cm^{-1}$ per Trp) and Tyr (ε_{280} = 1280 $M^{-1}.cm^{-1}$ per Trp). CD spectra were recorded on a JASCO J-810 Spectropolarimeter with a temperature controller module JASCO PFD-425S. Raw CD melting curves were implemented in OriginPro 9.0 (Originlab Corporation, U.S.A.) and fitted to a nonlinear fitting square routine protocol described elsewhere.[SI6] NMR samples were prepared by dissolving the freeze-dried peptide (~ 1-2 mg) in mixtures of phosphate buffer (50 mM, pH 6.5) or water and D_2O or DMSO-d_6 using 2,2-dimethyl-2-silapentane-5-sulfonate (DSS) as internal standard for chemical shifts (0 ppm). All spectra were recorded at 291 K (18 ^oC) on a Varian Mercury500 (500 MHz) spectrometer and processed using the Vnmrj 4.2 software. Inhibitor solutions (0.01-100 µM) and blank (DMSO/PBS buffer solution) were prepared for the PD-1 immunoblocking assay.

1. Summary of Contact Interactions from 3 Different Crystal Structures of PD-1: Pembrolizmab-Fab Complexes

Reported PDB codes of pembrolizumab-Fab complexed with human Programmed Cell Death protein 1 (PD-1) structures are 5JXE,[SI7] 5B8C[SI8] and 5GGS.[SI9] Those crystals structures are formed by di-, tetra- and dimeric assemblies, respectively. In each crystal, the monomer displaying the largest number of contact interactions was selected for analysis, and supplemental interactions found inside other monomers were also included if the residues were not found to be conformational outliers. The Ligplot+ software allowed for hydrogen bonds interpretation using a cut-off for maximum $H_{ydrogen}$-$A_{cceptor}$ distance of 2.70 Å, for salt bridges using a cut-off for maximum D_{onor}-$A_{cceptor}$ distance of 4.0 Å, and for hydrophobic contacts a minimum distance of 2.90 Å and a maximum distance of 3.90 Å. The corresponding wwPDB X-ray structure validation reports generated from https://www.wwpdb.org for each crystal (5JXE, 5B8C and 5GGS) were used to identify steric outliers interactions (**Table S1**). Residues presenting a mean B-factor higher than the B-factor high-median value of the entire monomeric protein were removed from consideration. The summary of contact polar and hydrophobic interactions are reported in **Table S2** and **Table S3** respectively.

Table S1. Steric clash interactions removed from crystallographic analysis consideration

PDB	Hydrophilic	Hydrophobic
5JXE	Ser^{87}:Tyr^{H35}	Ser^{87}:Tyr^{H35} ; Gly^{90}:Gly^{H57}
5B8C	-	Val^{64}:Phe^{H103}
5GGS	Arg^{86}:H_2O^{L304}:Tyr^{L36}	-

Binding Interface Summary.

In brief, **epitope-1** formed by residues of the $_{PD1}$CC' hairpin (Asn^{66}, Tyr^{68}, Gln^{75} (only in 5B8C) Thr^{76}, Asp^{77} and Lys^{78}) was found to interact with residues from the CDR-H1 (Thr^{H30}, Tyr^{H33}), CDR-H2 (Asn^{H52}, Ser^{H54}, and Asn^{H55}), and CDR-H3 (Tyr^{H101}, Arg^{H102}). This localized patch of residues contains a large hydrophobic core forming the hinge region of the PD1 curvature.

Epitope-2 ($_{PD1}$C'D loop [Phe^{82} – Phe^{95}]) was mapped and was found to display a number of interactions with the CDRs H1-3 and CDR-L1,3. Overall, Asp^{85} was shown to create a salt bridge with Arg^{H99}, while residues Ser^{87} and Gly^{90} hydrogen bonded to Arg^{H99} and Thr^{H58} respectively. Residue Glu^{84} was shown to create contacts with Tyr^{L36}, and Ser^{L95} (only in 5GGS), and strong hydrogen bonds between Arg^{86}:Asn^{H59}, Gln^{88}:$Asp^{H52,H55,H59}$, Pro^{89}:$Asp^{H52,H55}$, and Gln^{91} with Thr^{H58} and Asn^{H59} (only in 5GGS). Those hydrogen bonds mainly involved the backbone amides of the C'D loop residues with the CDR-H2 of pembrolizumab through water molecules.

Finally, **epitope-3** is composed of large patches from the $_{PD1}$BC and $_{PD1}$FG loops and residue Val^{64} from the C strand that generate a large surface of contacts with the CDR-L1,2 and CDR-H3 sections of pembrolizumab. Overall, hydrogen-bond contacts from Leu^{128}:Tyr^{L53}, Ala^{129}:Leu^{L58} and a salt bridge Lys^{131+}:Glu^{L59-} (CDR-L2), and 3 other hydrogen bonds from Lys^{131} and Ala^{132} to Tyr^{L53}, Arg^{H102}, Met^{H105} and Asp^{H108} (CDR-H3) accounted for this epitope. Interestingly, we found that the corresponding paratope-3 is highly lipophilic (~10 van der Walls contacts) due to a segment of the CDR-L2 rich in leucine and tyrosine residues (Tyr^{L53}, Leu^{L54}, Tyr^{L57}, and Leu^{L58}) in addition to Tyr^{L34} from the CDR-L1.

Table S2. Hydrophilic interactions between pembrolizumab-fab and PD-1

	PD-1	5JXE (B)		5B8C (C)		5GGS (Z)	
		HC (D)	LC (C)	HC (B)	LC (A)	HC (A)	LC (B)
BC loop	S60†				Y34‡		
	E61†				Y57‡		
	S62‡						G33†*, Y57‡*
CC' hairpin	F63†				Y34‡		Y34‡
	N66‡†	R102†		R102†		R102†	
	Y68‡			R102‡		Y101‡*	
	Q75‡			T30‡			
	T76†‡	Y101‡		Y101‡*, R102‡*		T30†*, Y101‡	
	D77‡	S54‡		S54‡, N55‡*		S54†*	
	K78†‡	Y101†*		Y33‡, N52‡*, Y101†		Y33‡, N52‡*, S54‡*, Y101†	
C'D loop	E84†						Y36‡*, S95†*
	D85‡	R99‡		R99‡, D104†*		R99‡, D104†*	
	R86†			N59‡*		N59‡*	S95†*, R96†*
	S87‡†	R99‡	S95‡	Y35‡, N59‡, R99‡		Y35‡, N59‡, R99‡	S95†*
	Q88‡†			N52‡*, N55‡*, N59‡*		N52‡*, N55‡*, N59‡*	
	P89†			N52‡*, N55‡*		N52‡*, N55‡*	
	G90†	T58†		N52‡*, N55‡*, T58†		N52‡*, N55‡*, T58†*	
	Q91‡†					T58†*, N59‡*	
DE hairpin	Q99‡				S32‡*		
FG loop	L128†		Y34‡		Y53‡		Y53‡
	A129†						Y53‡*, L58†*
	K131†‡			D108‡*	Y53‡*, E59‡	M105†, D108‡*	E59‡
	A132†				Y53‡*	R102‡	
G sheet	E136‡			Y101‡*, R102‡*		Y101‡*	

Residues interactions are marked with † for backbone, ‡ for side chain, and * through a water molecule. In red, the residues participating in a salt bridge.

Table S3. Lipophilic interactions between pembrolizumab and PD-1

	PD-1	5JXE (B)		5B8C (C)		5GGS (Z)	
		HC (D)	LC (C)	HC (B)	LC (A)	HC (A)	LC (B)
BC loop	T59				Y34		
	S60				Y34		
	E61				G33, Y34, Y57		
	S62						Y34, Y57
CC' hairpin	F63				Y34		Y34
	V64	F103			Y34	F103	
	N66	R102		R102		R102	
	Y68	R102		Y101, R102		Y101, R102	
	Q75			T28, T30			
	T76	Y101		Y101		Y101	
	D77	S54		S54			
	K78	Y33, R102, Y101		Y33, Y101, R102		Y33, Y101, R102	
	F82				S32		
C'D loop	P83		S32, Y34, Y36	F103	S32, Y34, Y36	F103	Y34, Y36
	D85	R99		R99		R99	
	R86		S95, R96, L98		R96, D97, L98		R96
	S87	N59, R99	S95	Y35, N59, R99, L100		Y35, N59	
	Q88	Y33, N59		Y33, N59		Y33, N59	
	P89	Y33, G50, I51, N52, G57, T58, N59		Y33, Y35, G50, I51, N52, G57, T58, N59		Y33, Y35, G50, I51, N52, G57, T58, N59	
	G90	T58		G57, T58		G57, T58	
F sheet	I126	R102					
	S127		Y34				
FG loop	L128		Y57	F103	Y34, Y53, L54		Y34, Y53, L54
	A129				Y53, Y57		
	P130				Y53, Y57, L58		
	K131			D108	L50, E59, S60	M105	Y53, E59
	A132			D100, R102, M105		R102	
G sheet	I134			R102		R102	

2. Paratopes – Epitopes Mapping

For each crystal representative of the PD-1:pembrolizumab binding (5JXE, 5B8C and 5GGS), the 3 PD-1 epitopes were determined graphically as patches of spatially close residues and partitioned (**Figure S1**). Mapping from the sum of contacts in **Tables S2/S3** then allowed us to determine the corresponding paratopes which are presented in **Table S4.**. Epitope-1 was therefore delineated from residues Asn^{66} to Lys^{78} localized on the $_{PD\text{-}1}$CC' β-hairpin, epitope-2 was delineated from residues Pro^{84} to Gln^{91} localized on the $_{PD\text{-}1}$C'D loop and epitope-3 formed of 3 segments from the $_{PD\text{-}1}$BC loop residues Thr^{69} to Phe^{63}, one residue from the C strand Val^{64} and a patch of residues Leu^{128} to Ile^{134} from the $_{PD\text{-}1}$C'D loop.

Table S4. Summary of Epitopes and Paratopes with polar and VdW contacts from the PD-1:pembrolizumab interface

Crystals	PD-1 ***Epitopes***	Pembrolizumab-Fab ***Paratopes***
5JXE	1. Asn^{66}, Tyr^{68}, Thr^{76}, Asp^{77}, Lys^{78} (CC' hairpin) 2. Asp^{85}, Arg^{86}, Ser^{87}, Gln^{88}, Pro^{89}, Gly^{90} (C'D loop) 3. Val^{64}, Ile^{126}, Ser^{127}, Leu^{128} (C strand + FG loop)	1. Tyr^{H33}, Ser^{H54}, Tyr^{H101}, Arg^{H102} (HCDR1-3) 2. Tyr^{H33}, Tyr^{H35}, Gly^{H50}, Ile^{H51}, Asn^{H52}, Gly^{H57}, Thr^{H58}, Asn^{H59}, Arg^{H99} | Ser^{L95}, Arg^{L96}, Leu^{L98} (HCDR1-3+LCDR3) 3. Arg^{H102}, Phe^{H103} | Tyr^{L34}, Tyr^{L57} (HCDR3+LCDR1,2)
5B8C	1. Asn^{66}, Tyr^{68}, Gln^{75}, Thr^{76}, Asp^{77}, Lys^{78} (CC' hairpin) 2. Asp^{85}, Arg^{86}, Ser^{87}, Gln^{88}, Pro^{89}, Gly^{90} (C'D loop) 3. Thr^{59}, Ser^{60}, Glu^{61}, Phe^{63}, Val^{64}, Leu^{128}, Ala^{129}, Pro^{130}, Lys^{131}, Ala^{132}, Ile^{134} Glu^{136} (BC loop + C strand + FG loop + G sheet)	1. Thr^{H28}, Thr$^{H\ 30}$, Tyr^{H33}, Asn^{H52}, Ser^{H54}, Tyr^{H101}, Arg ^{H102} (HCDR1-3) 2. Tyr^{H33}, Tyr^{H35}, Gly^{H50}, Ile^{H51}, Asn^{H52}, Gly^{H57}, Thr^{H58}, Asn^{H59}, Arg^{H99}, Leu^{H100}, Asp^{H104} | Arg^{L96}, Asp^{L97}, Leu^{L98} (HCDR1-3+LCDR3) 3. Asp^{H100}, Tyr^{H101}, Arg^{H102}, Phe^{H103}, Met^{H105}, Asp^{H108} | Gly^{L33}, Tyr^{L34}, Leu^{L50}, Tyr^{L53}, Leu^{L54}, Tyr^{L57}, Leu^{L58}, Glu^{L59}, Ser^{L60} (HCDR3+LCDR1,2)
5GGS	1. Asn^{66}, Tyr^{68}, Thr^{76}, Asp^{77}, Lys^{78} (CC' hairpin) 2. Pro^{83}, Glu^{84}, Asp^{85}, Arg^{86}, Ser^{87}, Gln^{88}, Pro^{89}, Gly^{90}, Gln^{91} (C'D loop) 3. Ser^{62}, Phe^{63}, Val^{64}, Leu^{128}, Ala^{129}, Lys^{131}, Ala^{132}, Ile^{134} Glu^{136} (BC loop + C strand + FG loop + G sheet)	1. Thr^{H30}, Tyr^{H33}, Asn^{H52}, Ser^{H54}, Tyr^{H101}, Arg^{H102} (HCDR1-3) 2. Tyr^{H35}, Gly^{H50}, Ile^{H51}, Asn^{H52}, Gly^{H57}, Thr^{H58}, Asn^{H59}, Arg^{H99}, Phe^{H103}, Asp^{H104}| Tyr^{L34}, Tyr^{L36}, Ser^{L95}, Arg^{L96} (HCDR1-3+LCDR1,3) 3. Arg^{H102}, Phe^{H103}, Met^{H105}, Asp^{H108} | Gly^{L33}, Tyr^{L34}, Tyr^{L53}, Leu^{L54}, Tyr^{L57}, Leu^{L58}, Glu^{L59} (HCDR3+LCDR1,2)

Figure S1. Surface representation of the PD-1:pembrolizumab-Fab fragments complexes (PDB codes: 5JXE, 58BC and 5GGS). Views of the binding interface with the 3 pairs of epitopes and paratopes from the PD-1 on the left and pembrolizumab-Fabs on the right. Epitopes 1, 2 and 3 and the corresponding cognate paratopes from pembrolizumab (views rotated by 180º shown) are depicted in red, blue and green respectively. Polar residues forming stabilizing hydrogen bonds and salt bridges contacts at the interface are noted and numbered on the surface while the residues responsible for van de Walls contacts are only colored. Stripped colors illustrate regions of pembrolizumab that shared interacting contact residues with several epitopes of PD-1.

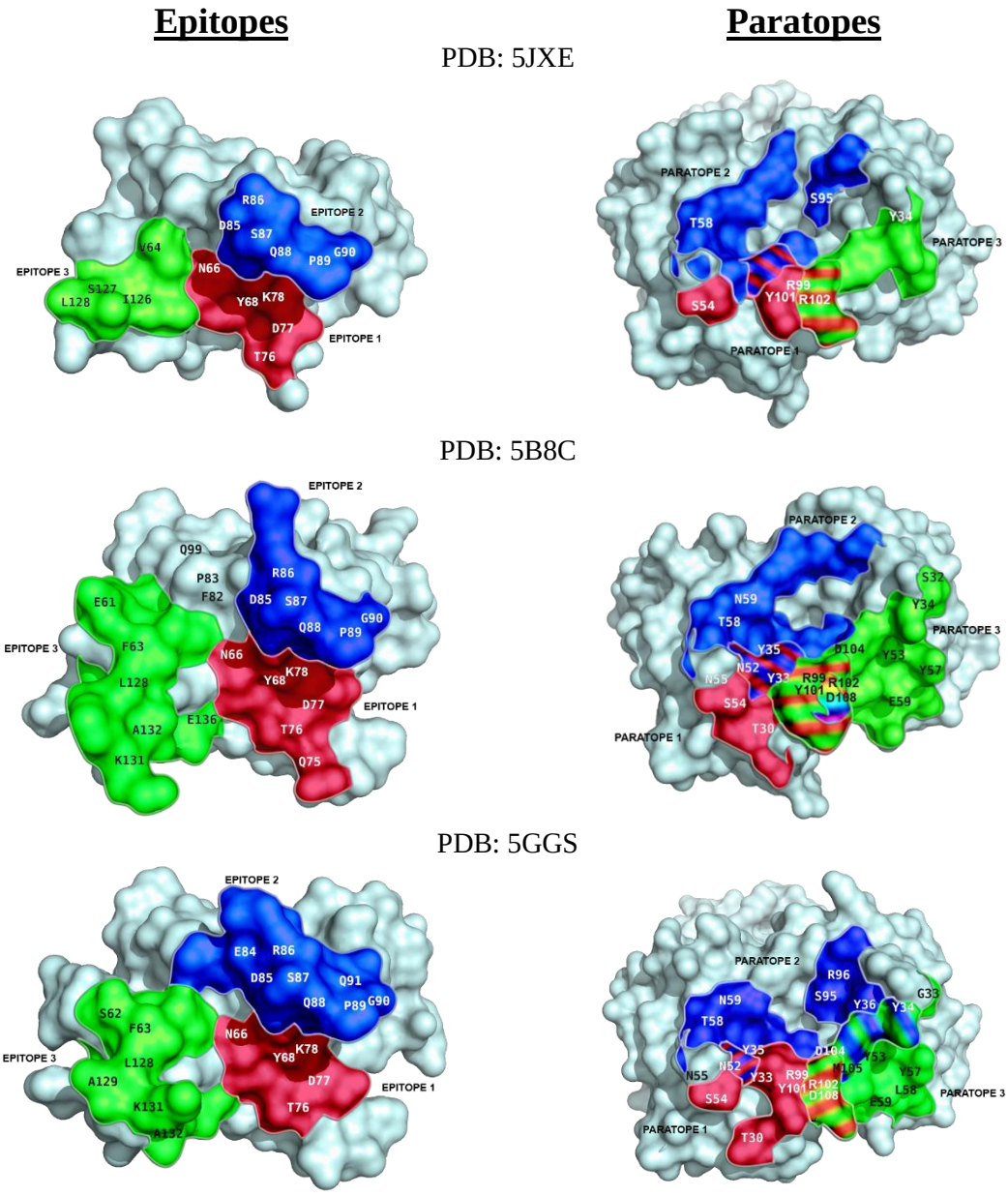

Figure *S*2. Binding mode from close-up views of pembrolizumab CAR-[RDYRFDMGFD]-YWG CDR-H3 at the interface with PD-1. (**A**) Overlay of pembrolizumab H3 loops [Arg^{H99} – Asp^{H108}] excised from co-crystal structures (PDB: 5JXE, 5B8C, 5GGS, in magenta) with the unbounded form (PDB: 5DK3, in blue), corresponding RMSD values of 0.38 Å, 0.26 Å, and 0.30 Å across backbone atoms calculated against the unbounded structure. (**B–D**) Ribbon representation of binding complexes from PDBs 5JXE, 5B8C and 5GGS are shown with PD-1 in cyan, and with the heavy and light chains of pembrolizumab in yellow and pink respectively. The network of contact interactions created by the H3 loop in each complex is depicted with H-bonds between H3 loop and PD-1 residues in magenta and green cyan respectively, and hydrophobic contacts in the same lighter colors. Direct and water mediated H-bonds are displayed with yellow and cyan dashed lines and salt bridges with red dashed lines.

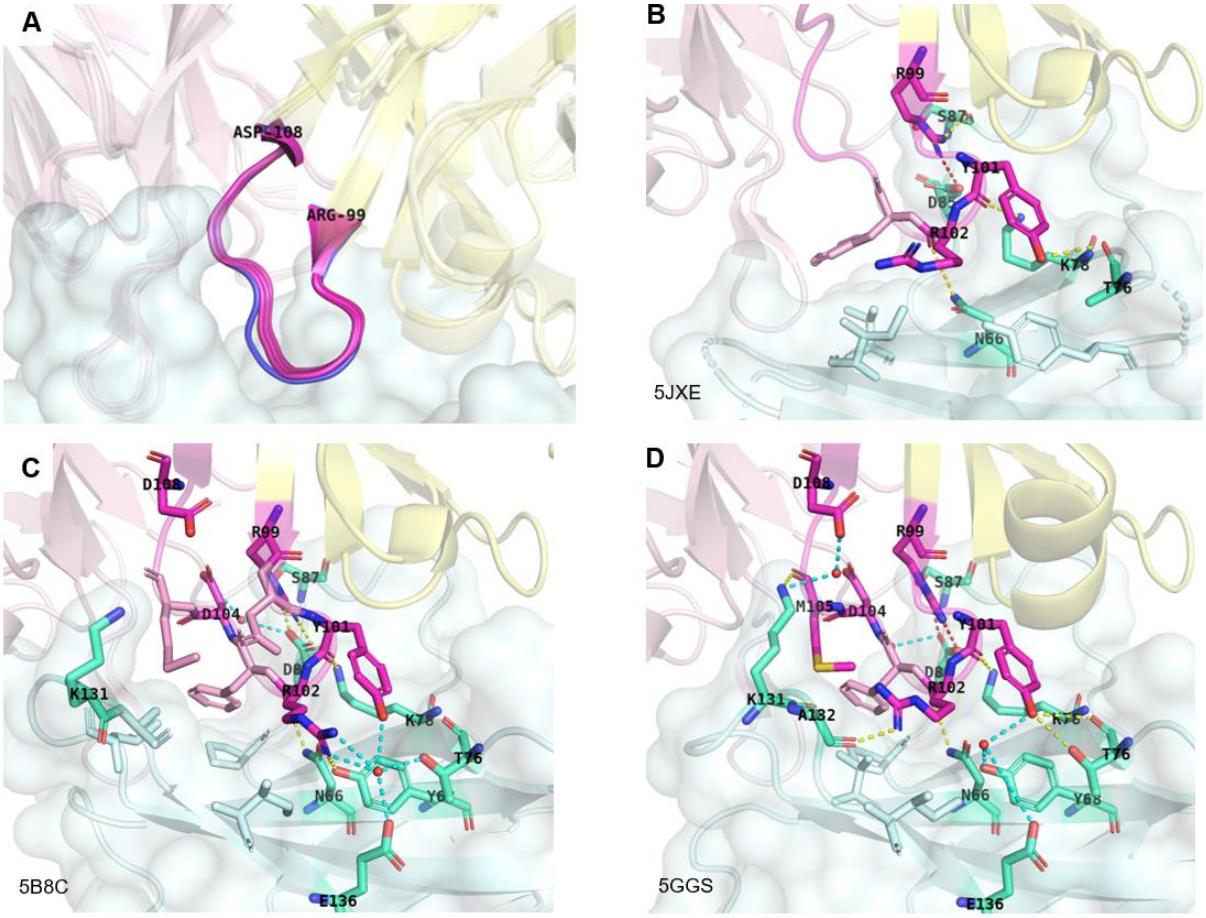

The buried surface area (BSA) at the contact interface between PD-1 and the pembrolizumab was calculated from the PD-1:pembrolizumab Fab co-crystal structure (PDB code: 5GGS) using the web-based software dr_SASA (Table S5).[SI10] Each subdomain of pembrolizumab (HCDR1 C22-Y33, HCDR2 I51-G56, and HCDR3 Y95-Q112) in contact with PD-1 was extracted from the full structure using PyMOL to generate individual PDB file. The individual PDBs were imputed in dr_SASA to calculate the buried surface areas of each HCDR1, HCDR2, and HCDR3. The total BSA involving pembrolizumab extend over 1,218 Å^2 (heavy and light chains), while the surface on PD-1 was calculated to 1,099 Å^2. The β-hairpin from the HCDR3 subdomain accounts for 460 Å^2 which represents 38% of the total BSA overall.

Table *S*5. BSA calculated for PD-1:pembrolizumab complex.

5GGS	PD-1	Light Chain	Heavy chain	HCDR1	HCDR2	HCDR3
BSA (Å^2)	1,099	503	715	126	130	460

Furthermore, the volume of the cavity formed at the surface of PD-1 by the motion of the C'D and FG loops to generate the groove of interactions with pembrolizumab was estimated using the web-based software POCASA 1.1. Again, the same PD-1:pembrolizumab Fab co-crystal structure (PDB code: 5GGS) was exploited for these calculations. The search for cavities was achieved on Chain Y while maintaining molecules of water present in the crystal, with the recommended parameters of 1 Å for the grid size, and an output of the top 5 cavities using a rolling sphere of 3 Å radius. Using a 3-Å radius probe, only 3 small pockets of 174, 133, and 26 Å^3 volume respectively were detected on the surface of PD-1 (Figure S2). By increasing iteratively the size of the probe by 1 Å radius, shallower and wider cavities were identified. While using a 4-Å radius probe did not drastically alter the initial results, a 5-Å radius probe revealed a new cavity in the groove between the C'D and FG loops, and the back CC' loop. Even though the cavity is more shallow and wide the volume was calculated to 229 Å^3. When using a sphere of 6-7 Å radius, results were comparable with a groove volume estimated to 368-372 Å^3 while the other cavities at the surface of PD-1 remain also mainly unchanged (cav. A 154-156 Å^3, and cav. B 145-157 Å^3). Overall the calculations with POCASA 1.1. using a large radius sphere (6-7 Å) were found optimum to estimate the volume of the shallow binding groove on PD-1 (370 ± 2 Å^3) corresponding to the buried surface of contacts with the HCDR3 loop of pembrolizumab.

Figure *S*3. Volume calculations of binding cavities at the surface of PD-1. (PDB code: 5GGS). Views of the predicted binding cavities using a probe of various radius: **A.** 3 Å; **B.** 5 Å; **C.** 6 and 7 Å; **D.** 6 Å and an overlay with the CDR-H3 loop (deep red).

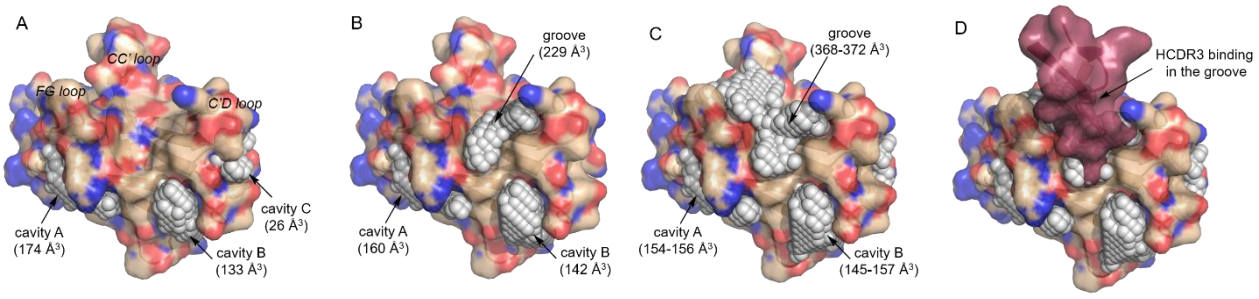

3. Plasticity of the PD-1 C'D loop in binding PD-L1 vs pembrolizumab-fab visualized by morphing simulations

As shown in Figure S3A, PD-L1 binds to PD-1 mainly through epitope-1 (CC' β-hairpin), leaving epitope-2 unengaged and highly disordered due to the flexibility of the long $_{PD\text{-}1}$C'D loop. On the contrary, upon binding to pembrolizumab, the $_{PD\text{-}1}$C'D loop becomes fully extended to generate a groove at the interface with both heavy and light chains of pembrolizumab via a number of polar contacts (Figure S3B).

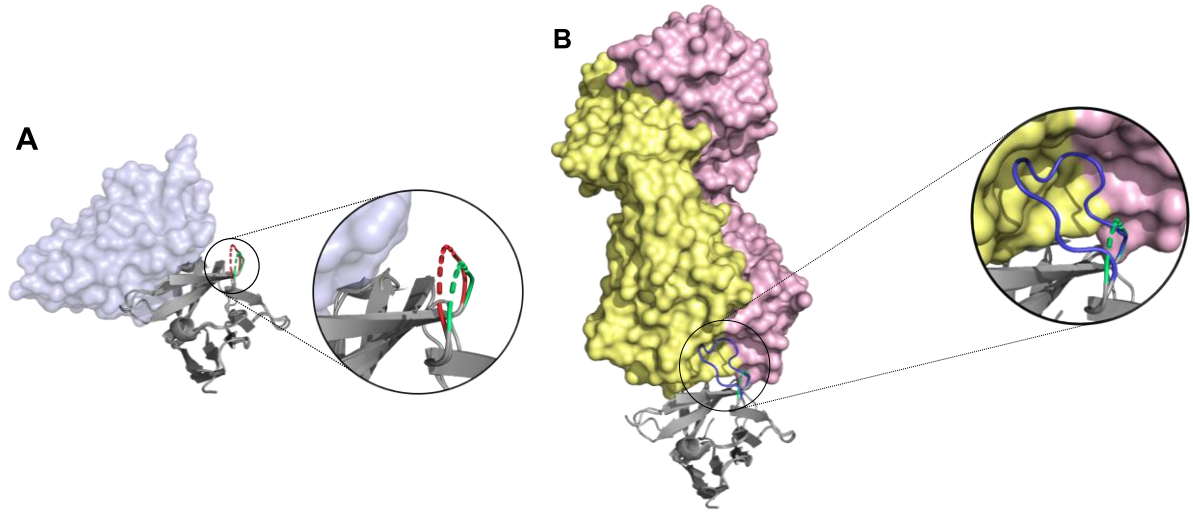

Figure *S*4. Variable Motion of the PD-1 C'D loop upon binding to PD-L1 or pembrolizumab. A. Close-up view of the disordered residues [83-93] of the $_{PD\text{-}1}$C'D loop by the superimposition of 2 crystal structures (PDBs: 4ZQK/3RRQ). Ribbon representation of the *apo*-PD1 C'D loop in green (3RRQ) and the same C'D loop of PD-1 bound to PD-L1 in red (4ZQK). **B.** Close-up view of the $_{PD\text{-}1}$C'D loop in blue bounded to pembrolizumab-Fab residues (5GGS), and the $_{PD\text{-}1}$C'D loop from *apo*-PD1 (green) for comparison. Surface of pembrolizumab heavy-chain is illustrated in yellow and light-chain in pink.

Morphing Simulations. Because of two undefined segments in the original *apo*-PD-1 crystal file (PDB: 3RRQ), a remodeling of the C'D loop and insertion of residue E61 were required prior to interpretation. Using the UCSF Chimera Software and the MODELLER add-on,[SI3] a portion of the C'D loop of PD-1 [Pro^{83} – Arg^{94}], formed by the sequence of residues D^{85}RSQPGQD^{92} was remodeled to obtain a set of 500 low-energy conformers generated using the loop modeling protocol: DOPE-HR (Figure S4A). The lowest-energy loop conformer was selected using the zDOPE score related to free energy (zDOPE -1.93 au) which enabled us to obtain an initial wild-type PD-1 model with a reconstituted C'D loop (PDB: 3RRQ*). Secondly, the missing E61 residue was added with InteractiveROSETTA (KIC protocol > SES loop modeling, *De Novo*) to generate the complete model of the wild-type *apo*-PD-1(PDB: 3RRQ**) bearing the reconstituted C'D and BC loops shown in Figure S4B.[SI4]

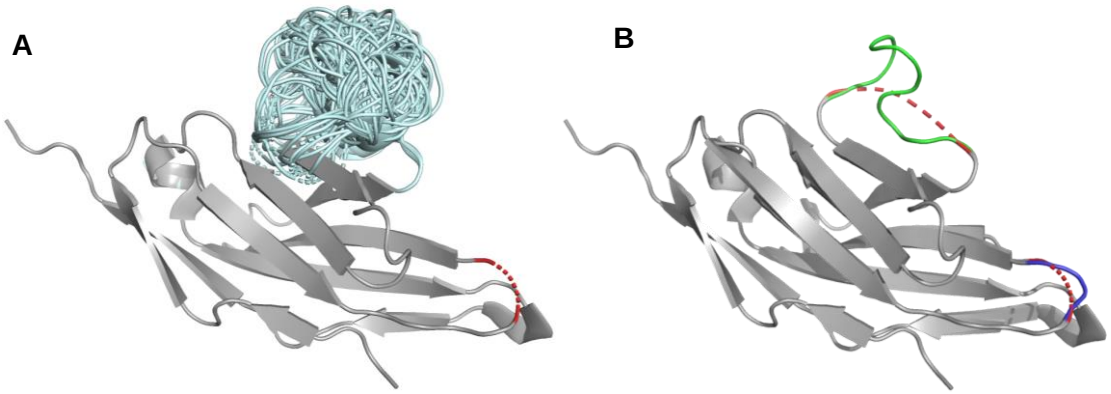

Figure S5. Remodeling of the PD-1 C'D loop of 3RRQ into 3RRQ A.** Overlay of the 500 lowest-energy loop conformers minimized with Chimera; **B.** Overlay of the *apo*-PD1 crystal structure 3RRQ and the final computed model 3RRQ**. In red dashed lines are the original loops and in green and blue are the remodeled section [Asp^{85} – Asp^{92}] of the C'D loop, and the BC loop E61 residue respectively.

Having in hand both remodeled *apo*-PD-1 (PDB: 3RRQ**) and bounded PD-1 to pembrolizumab (*e.g.* PDB: 5GGS) structures, a morphing simulation was achieved to extrapolate the plausible trajectory of PD-1 upon binding. The new PD-1 model (PDB: 3RRQ**) along with the *apo*-pembrolizumab (PDB: 3DK3) were overlaid with the reported PD-1:pembrolizumab-Fab X-ray complex (PDB: 5GGS) (RMSD = 0.41 Å and 0.74 Å respectively, Figure S4, STEP 1). Interpolated trajectories were calculated on each individual chain/object (pembrolizumab heavy-chain, light-chain and PD-1 separately) to obtain a conformational simulation from the *apo*-forms to the bounded states through a motion comprising 60 states (60 refinement cycles, STEP 2). The 3 objects were reassembled together to obtain the full-length simulation with the motion of both pembrolizumab and PD-1 (Supplementary Video S3) and water molecules from the 5GGS crystal were added to the final file to maintain the hydrogen bond and salt bridge contacts involving water (STEP 3). Dynamic polar interactions between the two proteins are displayed in the final state to generate the Supplementary Video S3.

Figure S6. Representative protocol for building a binding complex in a morphing simulation. Steps to generate the simulation from the open conformation of PD-1 (PDB: 3RRQ**) and the apo-pembrolizumab-fab (PDB: 3DK3) to the closed conformation in the drug-receptor complex (PDB: 5GGS).

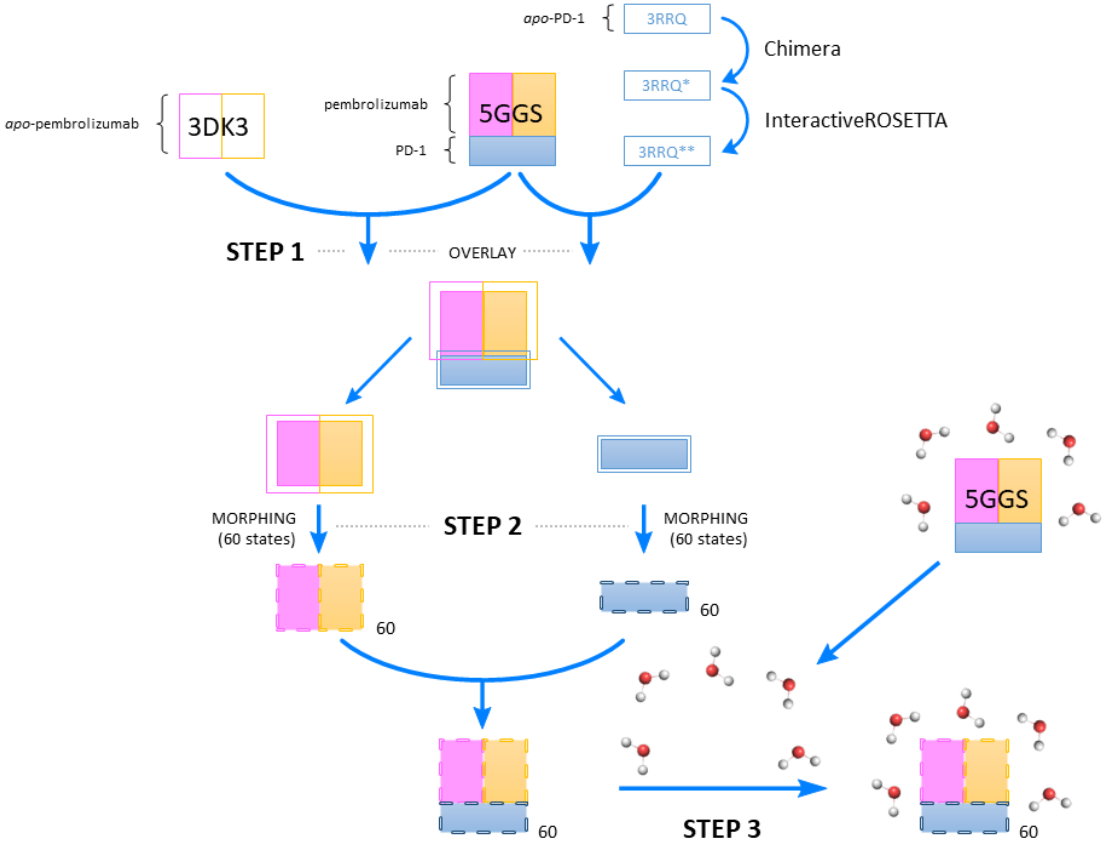

4. Loop dynamics from the PD-1 immunoreceptor by MD simulations

To better evaluate the plasticity of the PD-1 receptor, both structures of remodeled *apo*-PD-1 (PDB: 3RRQ**) and the PD-1 excised from PDBs 5GGS and 5B8C have been tested for loop flexibility using the ToeLoop software.[SI5] The MD simulations obtained from ToeLoop gave an interesting estimate of the different loops flexibility (Figure S7). The results obtained for the *apo*-PD-1 demonstrated that the $_{PD\text{-}1}$C'D loop [Phe^{82} – Phe^{95}] is a "fast" moving loop with high flexibility (red color <10 ns for the motion) while the $_{PD\text{-}1}$FG loop appeared less flexible (blue color). As expected, the same $_{PD\text{-}1}$C'D loop bounded to the pembrolizumab-Fab was predicted to loose complete flexibility upon binding (green color for motion > 500 ns). Overall, the largest allosteric change observed in PD-1 with the morphing simulation is supported by the flexibility of the $_{PD\text{-}1}$C'D loop on the nanosecond time-scale prior to binding and was found to acquire rigidity afterwards, mainly due to the additive strong hydrophilic interactions.

Figure S7. Temporal evaluation of the PD-1 loops motion. Protein loops were categorized as fast (**red**), slow (**blue**) and static (**green**) from a protein structure (PDB) according to their correlation time, i.e. faster than 10 ns, 10 to 500 ns, and slower than 500 ns respectively.[SI9] **A.** Unbounded state of PD-1 (3RRQ**); **B.** PD-1 bound to pembrolizumab-Fab (5B8C). The all-atom backbone RMSD of the C'D allosteric loop between the free and bound forms is 3.76 Å, whereas RMSD increases of 2.39 Å and 1.30 Å were found for epitope 1 and 3, respectively. The ribbon representations of PD-1 have been generated from the ToeLoop results using Pymol.

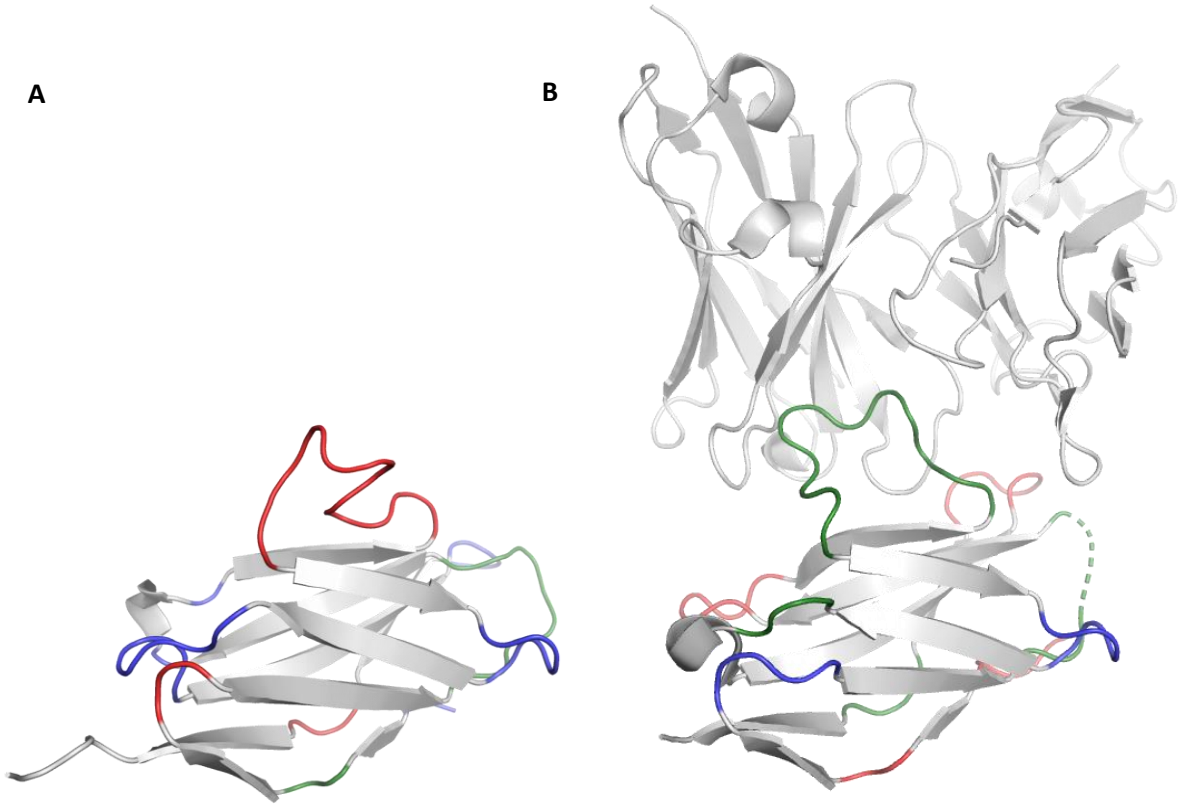

Finally, the $_{PD\text{-}1}$C'D loop *[Phe^{82} – Phe^{95}]* from PDBs 3RRQ**, 5GGS and 5B8C were compared in terms of geometry and size. It was found that even though the 3-dimensional structure of the loop is mainly a random coil, the distance between segment termini ($d_{Phe82\text{-}Phe95}$ = 11.7 Å) is about 2/3 of the longest Cα-Cα distances between residues across the loop ($d_{Pro83\text{-}Arg94}$ = 16.3 Å) which is characteristic of an Ω-type loop (Figure S8).

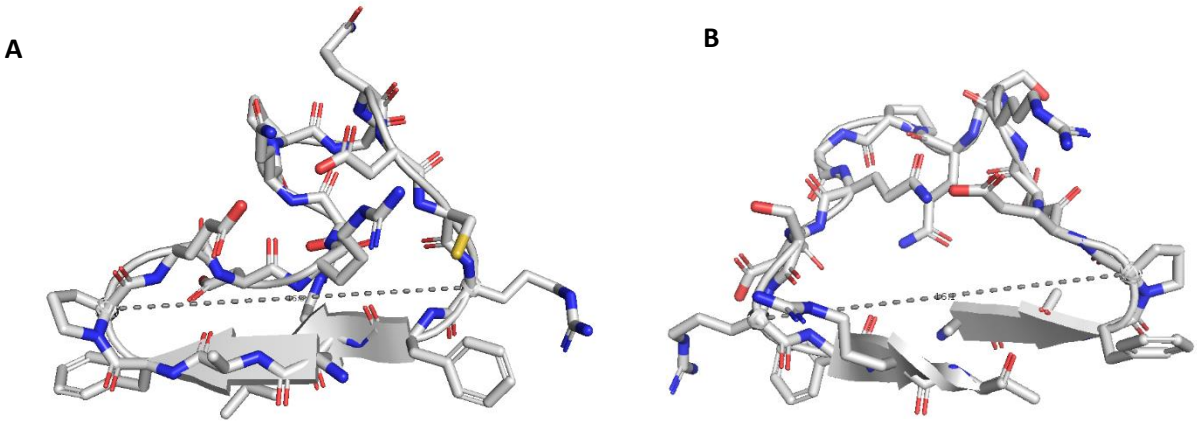

Figure S8. Structural evidence of a C'D loop forming a Ω-type loop. A. C'D loop from PDB 3RRQ** showed a longest internal distance of 16.9 Å, and **B.** C'D loop from PDB 3RRQ** showed a longest internal distance of 16.1 Å while in both cases the termini of the loop are at 11.7 Å. The ribbon representations of PD-1 and the distances have been generated using Pymol.

5. Peptide Synthesis, Purification, and Structural Characterization

a. Peptide Synthesis and Analysis.

General procedure for peptide synthesis *via* Fmoc-SPPS: Syntheses were carried out at room temperature in anhydrous DMF using the resin described in general information (200 to 300 mg, 1.0 eq., as reported below for each peptide) by successive iterations of deprotection/coupling. Vials of each Fmoc-protected α-amino acid (4.0 eq.) were prepared with HBTU (4.4 eq.) and HOBt (4.4 eq.) neat. For each iteration, the deprotection/coupling sequence entails: (1) Wash of the resin with DMF (3 X 5.0 mL) for 0.5 min each, (2) Fmoc-deprotection run twice using an excess of piperidine in DMF (20% v/v, 5.0 mL) for 5 mins each, (3) Wash with DMF (6 X 5.0 mL) for 0.5 min each, (4) The cocktail from the entire vial (described above) was dissolved with *N*-methylmorpholine in DMF (3.0 mL, 4 M) and added for a 40-min coupling, (5) Wash with DMF (3 X 5.0 mL) for 0.5 min each, finalized the sequence. After the final *N*-terminal coupling a final Fmoc-deprotection was achieved (step 2). Resulting peptides attached to the resin were washed with CH_2Cl_2 (2 X 10 mL), and the resin was dried under vacuum before storage under argon at -78 ^oC until cleavage.

General procedure for peptide cleavage from resins: a protocol of simultaneous Wang resin cleavage and side-chains' deprotection was applied. The dried resin was suspended in a cleavage cocktail (TFA/thioanisole/EDT/anisole, 90:5:3:2 v/v, 1.0 mL per 20 mg of resin) and shaken for 1.5 h at RT. The mixture was filtered to remove the resin and the mother liquor was evaporated on a rotary evaporator. The crude peptides (~250 mg) were precipitated in cold ether (40 mL), then centrifuged and washed with cold ether (3 X 40 mL). The resulting crude peptides were solubilized in water and lyophilized before being stored as dry powders under argon at -78 ^oC.

All lyophilized crude peptides were analyzed by analytical reverse-phase high-performance liquid chromatography (RP-HPLC) on a Hitachi L-7000 series equipped with a XBridge BEH C_{18} column (130 Å, 10 µm, 4.6 mm x 250 mm). HPLC grade acetonitrile and deionized water, each containing 0.1% trifluoroacetic acid, were used as mobile phases for analytical and semi-preparative RP-HPLC. Each peptide was analyzed using a gradient from 10% to 50% of acetonitrile over 30 mins with a flow rate of 1.0 mL/min at room temperature and a detection at 220 nm. Yields refer to chromatographically and spectroscopically pure compounds. All peptides were purified with a Hitachi L-7000 series HPLC equipped with a semi-preparative XBridge BEH C_{18} column (130 Å, 10µm, 10 mm x 250 mm) stationary phase by scaling up the analytical conditions. Pure fractions of peptides were collected and analyzed by analytical RP-HPLC and mass spectrometry using a Microflex LRF matrix-assisted laser desorption ionization time-of-flight (MALDI-TOF) instrument.

b. Peptide characterization by MALDI-TOF MS and RP-HPLC.

Table S6. Summary of peptide sequences **1a-e, 2a-c** prepared in this study

Peptides	Sequences	Similarity to CDR-H3 loop	Hairpin %-fold (χ_F) 293K
1a	**RW**CAR-GGGGKKGGFD-YWG**WE**	- -	Random coil
1b	RGVAR-RDYRGD**P**GFD-YWVWE	-	Random coil
1c	**RW**CAR-RDYRFDMGFD-YWG**WE**	*native*	0%
1d	**RW**VAR-RDYR**G**DMGFD-YWV**WE**	+	91 ± 1%
1e	**RW**VAR-RDYRFDMGFD-YWV**WE**	+ +	55 ± 1%
2a	**RWVW**-GGGGKKGGGG-**WVWE**	- -	87 ± 1%
2b	**RWVW**-RDYR**G**DMGFD-**WVWE**	+	81 ± 1%
2c	**RWVW**-RDYRFDMGFD-**WVWE**	+ +	54 ± 1%

Table S7. Summary of peptides **1a-e, 2a-c** synthesis and purity quantification

Peptides	Isolated Yield (%)[a]	HPLC Purity[b]	(m/z) $[M+H]^+$		(m/z) $[M+Na]^+$	
			Calcd	Found[c]	Calcd	Found[c]
1a	41	98%	2273.04	2273.50	2295.03	2295.45
1b	33	98%	2538.18	2538.17	-	-
1c	33	90%	2715.18	2715.31	-	-
1d	34	>99%	2663.24	2663.64	-	-
1e	36	>99%	2753.28	2753.87	2775.26	2774.83
2a	70	92%	1958.97	1958.63	1980.96	1980.76
2b	35	99%	2459.11	2459.39	2481.09	2481.35
2c	30	93%	2549.16	2549.59	-	-

[a] Yields obtained after purification by semi-preparative RP-HPLC [b] Determined by peak integration detected by UV-absorbance at 220 nm from the purified lyophilized peptide samples. [c] Determined by MALDI-TOF mass spectrometry.

Peptide **1a**: RWCAR-GGGGKKGGFD-YWGWE

Wang resin (300 mg, 132 μmol) was used to prepare **1a** according to the general procedure for peptide synthesis. After the general procedure for peptide cleavage from resins, 206 mg of crude peptide was obtained. Crude peptide **1a** (80 mg) was purified by semi-preparative RP-HPLC giving **1a** (48 mg, 21 μmol) in 41% yield.

Analytical HPLC: Peptide **1a** retention time t_R = 19.65 min with a purity of 98%.

t_R (min)	Area (mAU*min)	Area (%)
19.65	22700160	98
24.32	371240	2

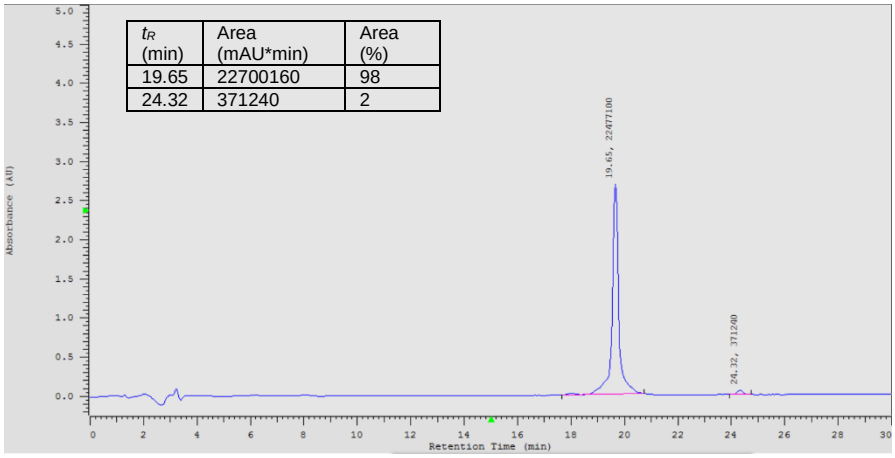

Peptide **1b**: RGVAR-RDYRGDPGFD-YWVWE

Wang resin (300 mg, 132 μmol) was used to prepare **1b** according to the general procedure for peptide synthesis. After the general procedure for peptide cleavage from resins, 395 mg of crude peptide was obtained. Crude peptide **1b** (370 mg) was purified by semi-preparative RP-HPLC giving **1b** (112 mg, 44 μmol) in 33% yield.

Analytical HPLC: Peptide **1b** retention time t_R = 18.83 min with a purity of 98%.

t_R (min)	Area (mAU*min)	Area (%)
17.87	204894	2
18.83	12428345	98

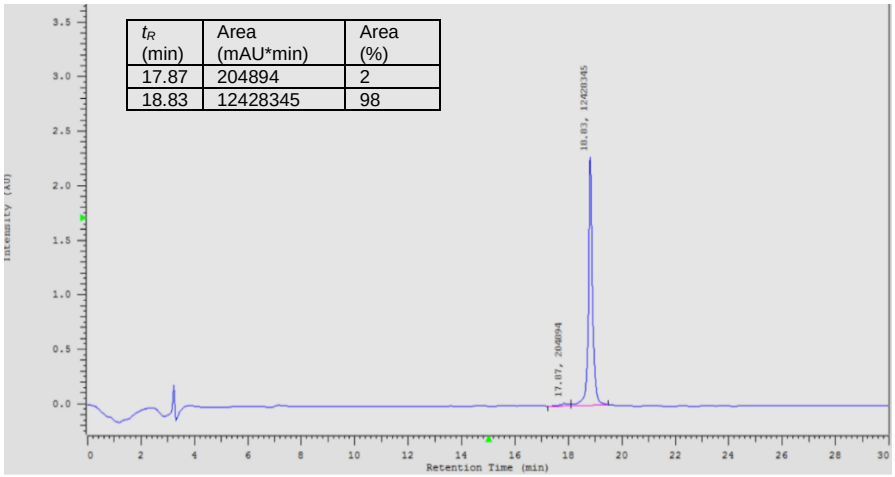

Peptide **1c**: RWCAR-RDYRFDMGFD-YWGWE

Wang resin (300 mg, 132 μmol) was used to prepare **1c** according to the general procedure for peptide synthesis. After the general procedure for peptide cleavage from resins, 434 mg of crude peptide was obtained. Crude peptide **1c** (60 mg) was purified by semi-preparative RP-HPLC giving **1c** (16 mg, 6 μmol) in 33% yield.

Analytical HPLC: Peptide **1c** retention time t_R = 22.72 min with a purity of 90%.

t_R (min)	Area (mAU*min)	Area (%)
21.20	531456	4
22.27	677879	6
22.72	10384224	90

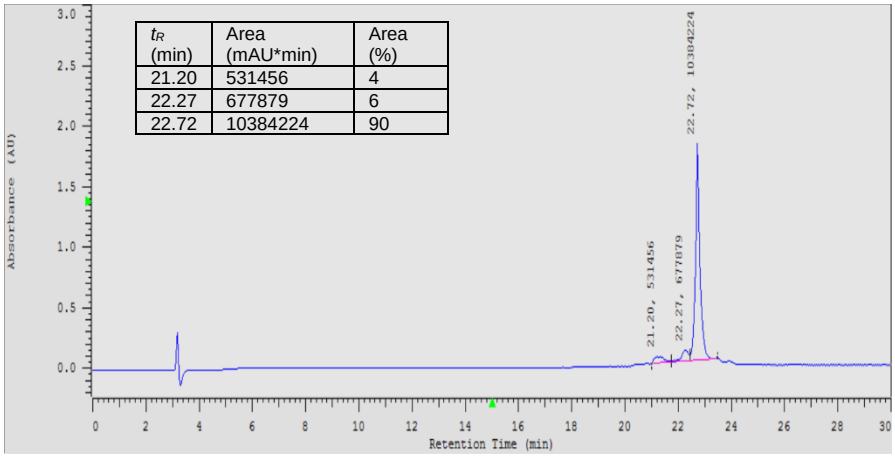

Peptide **1d**: RWVAR-RDYRGDMGFD-YWVWE

Wang resin (300 mg, 132 μmol) was used to prepare **1d** according to the general procedure for peptide synthesis. After the general procedure for peptide cleavage from resins, 480 mg of crude peptide was obtained. Crude peptide **1d** (80 mg) was purified by semi-preparative RP-HPLC giving **1d** (20 mg, 7 μmol) in 34% yield.

Analytical HPLC: Peptide **1d** retention time t_R = 21.47 min with a purity >99%.

t_R (min)	Area (mAU*min)	Area (%)
21.47	11388360	>99

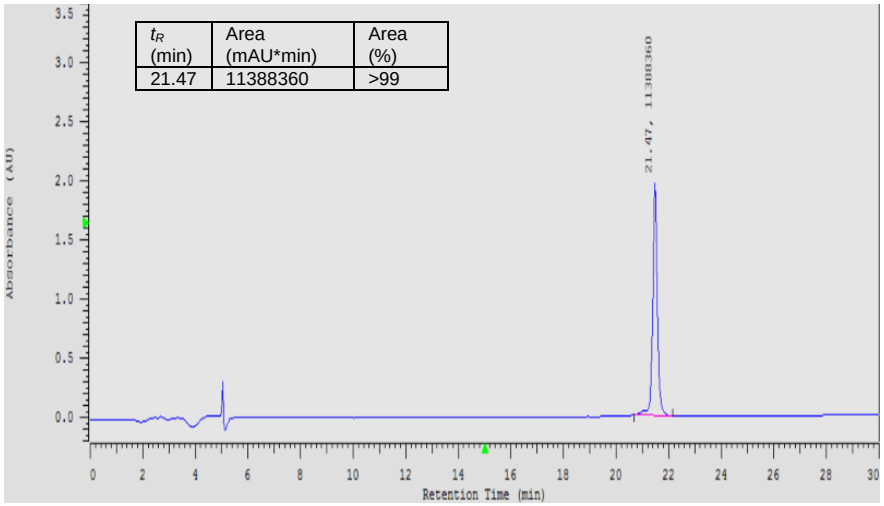

Peptide **1e**: RW-VAR-RDYRFDMGFD-YWV-WE

Wang resin (200 mg, 88 μmol) was used to prepare **1e** according to the general procedure for peptide synthesis. After the general procedure for peptide cleavage from resins, 204 mg of crude peptide was obtained. Crude peptide **1e** (80 mg) was purified by semi-preparative RP-HPLC giving **1e** (35 mg, 13 μmol) in 36% yield.

Analytical HPLC: Peptide **1e** retention time t_R = 23.12 min with a purity >99%.

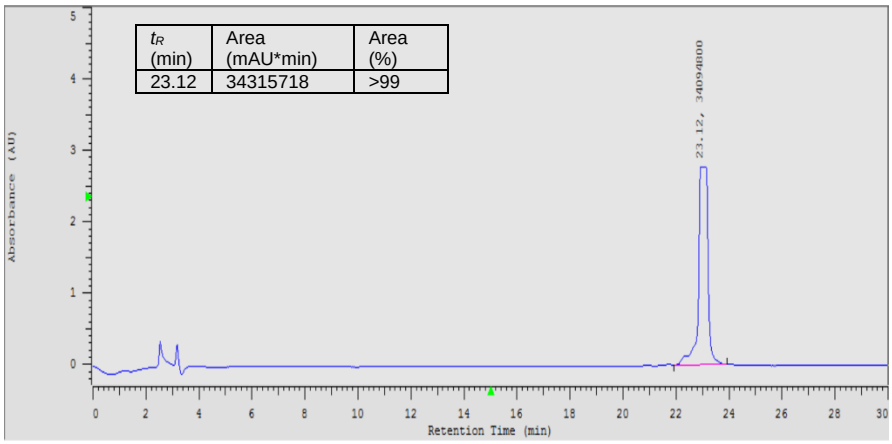

t_R (min)	Area (mAU*min)	Area (%)
23.12	34315718	>99

Peptide **2a**: RWVW-GGGGKKGGGG-WVWE

Wang resin (300 mg, 132 μmol) was used to prepare **2a** according to the general procedure for peptide synthesis. After the general procedure for peptide cleavage from resins, 244 mg of crude peptide was obtained. Crude peptide **2a** (100 mg) was purified by semi-preparative RP-HPLC giving **2a** (74 mg, 38 μmol) in 70% yield.

Analytical HPLC: Peptide **2a** retention time t_R = 17.63 min with a purity of 92%.

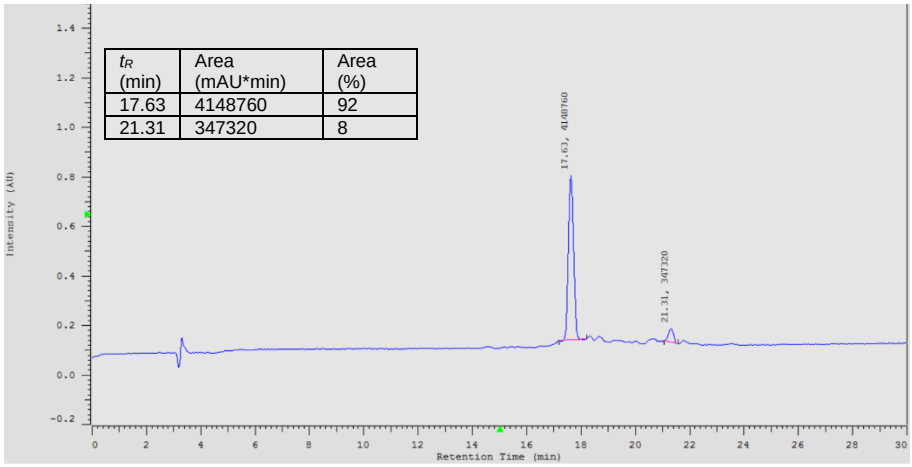

t_R (min)	Area (mAU*min)	Area (%)
17.63	4148760	92
21.31	347320	8

Peptide **2b**: RWVW-RDYRGDMGFD-WVWE

Wang resin (300 mg, 132 μmol) was used to prepare **2b** according to the general procedure for peptide synthesis. After the general procedure for peptide cleavage from resins, 224 mg of crude peptide was obtained. Crude peptide **2b** (100 mg) was purified by semi-preparative RP-HPLC giving **2b** (35 mg, 14 μmol) in 35% yield.

Analytical HPLC: Peptide **2b** retention time t_R = 23.20 min with a purity of 99%.

t_R (min)	Area (mAU*min)	Area (%)
22.59	260844	1
23.20	29909616	99

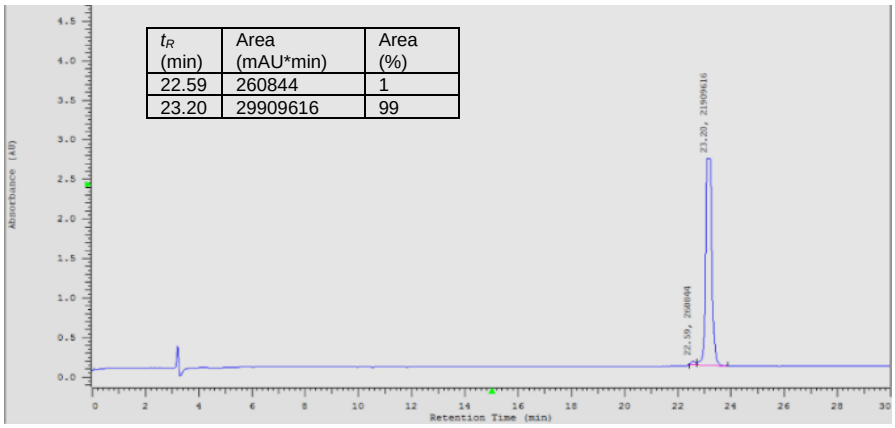

Peptide **2c**: RWVW-RDYRFDMGFD-WVWE

Wang resin (200 mg, 88 μmol) was used to prepare **2c** according to the general procedure for peptide synthesis. After the general procedure for peptide cleavage from resins, 111 mg of crude peptide was obtained. Crude peptide **2c** (80 mg) was purified by semi-preparative RP-HPLC giving **2c** (24 mg, 9 μmol) in 30% yield.

Analytical HPLC: Peptide **2c** retention time t_R = 25.15 min with a purity of 93%.

t_R (min)	Area (mAU*min)	Area (%)
24.45	2066768	7
25.15	27644950	93

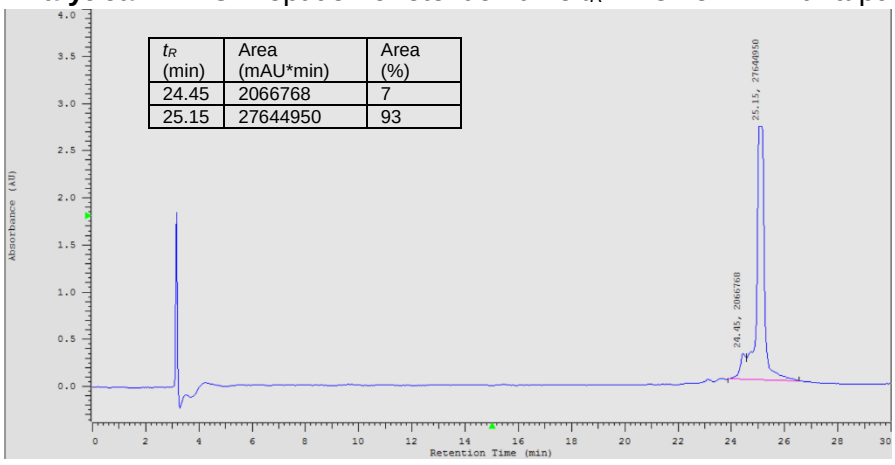

6. Characterization of Peptide Constructs by NMR and CD Spectroscopy

a. Thermodynamic Parameters of Folding Determined by Circular Dichroism Spectroscopy.

To determine the thermodynamic parameters characterizing the folding of each peptide construct based on their secondary structures, raw data of molar ellipticity [θ(T)] obtained by CD spectrum at 228 nm were fitted to Eq. S1 using the Gibbs-Helmholtz equation (Eq. S2) for a two-state model (folded/unfolded transition) accordingly to the reported procedure by N. J. Greenfield.[SI11] Raw melting curves of molar ellipticity as a function of temperature $[\theta(T)]_{228}$ were fitted following fitting protocol previously described[SI6] using the software OriginPro 9.0, to the following equation:

$$\theta(T) = \theta_U + (\theta_F - \theta_U)\frac{e^{-\frac{\Delta G(T)}{RT}}}{1+e^{-\frac{\Delta G(T)}{RT}}} \qquad \text{Eq. S1}$$

with

$$\Delta G(T) = \Delta H_m * \left(1 - \frac{T}{T_m}\right) - \Delta Cp * ((T_m - T) + T * \ln\left(\frac{T}{T_m}\right)) \qquad \text{Eq. S2}$$

$[\theta]_U$ and $[\theta]_F$ being the molar ellipticity values for the 100%-unfolded and 100%-folded states respectively, R being the ideal gas constant (R = 1.987 cal.mol^{-1}.K^{-1}), ΔH_m the enthalpy at the melting temperature T_m, and ΔC_p the specific heat capacity at constant pressure ($\Delta C_p < 0$ for a folding transition).[SI12]

Other thermodynamic parameters were calculated using OriginPro 9.0 based on the following equations:

$$\Delta H^o = \Delta H_m + \Delta Cp * (298 - T_m) \qquad \text{Eq. S3}$$

$$\Delta S^o = \frac{\Delta H_m}{T_m} + \Delta Cp * \ln\left(\frac{298}{T_m}\right) \qquad \text{Eq. S4}$$

$$\Delta G^o = \Delta H_m * \left(1 - \frac{298}{T_m}\right) - \Delta Cp * \left(T_m - 298 + 298 * \ln\left(\frac{298}{T_m}\right)\right) \qquad \text{Eq. S5}$$

$$T\Delta S^o = \left(\frac{\Delta H_m}{T_m} + \Delta Cp * \ln\left(\frac{298}{T_m}\right)\right) * 298 \qquad \text{Eq. S6}$$

The ΔH^o, ΔS^o, and ΔG^o values representing the standard enthalpy, entropy and free enthalpy of folding respectively at 298 K were calculated from the best-fit results in OriginPro 9.0 with their corresponding standard deviations. Standard deviation on temperatures were obtained from experimental data points recorded every 0.1 °C giving a standard deviation ΔT = 0.1 + 0.1*dT (dT as the error on the temperature calculated by the software).

A melting curve representing the evolution of the fraction of folding with the temperature (thermodynamic structural transition) was also plotted accordingly to the following equation:

$$x_F(T) = \frac{\theta(T) - \theta_U}{\theta_F - \theta_U} \qquad \text{Eq. S7}$$

With χ_F representing the fraction of folding at the temperature T.

Figure S9. CD spectra recorded as a function of temperature for peptides **1a-e** [a-e]

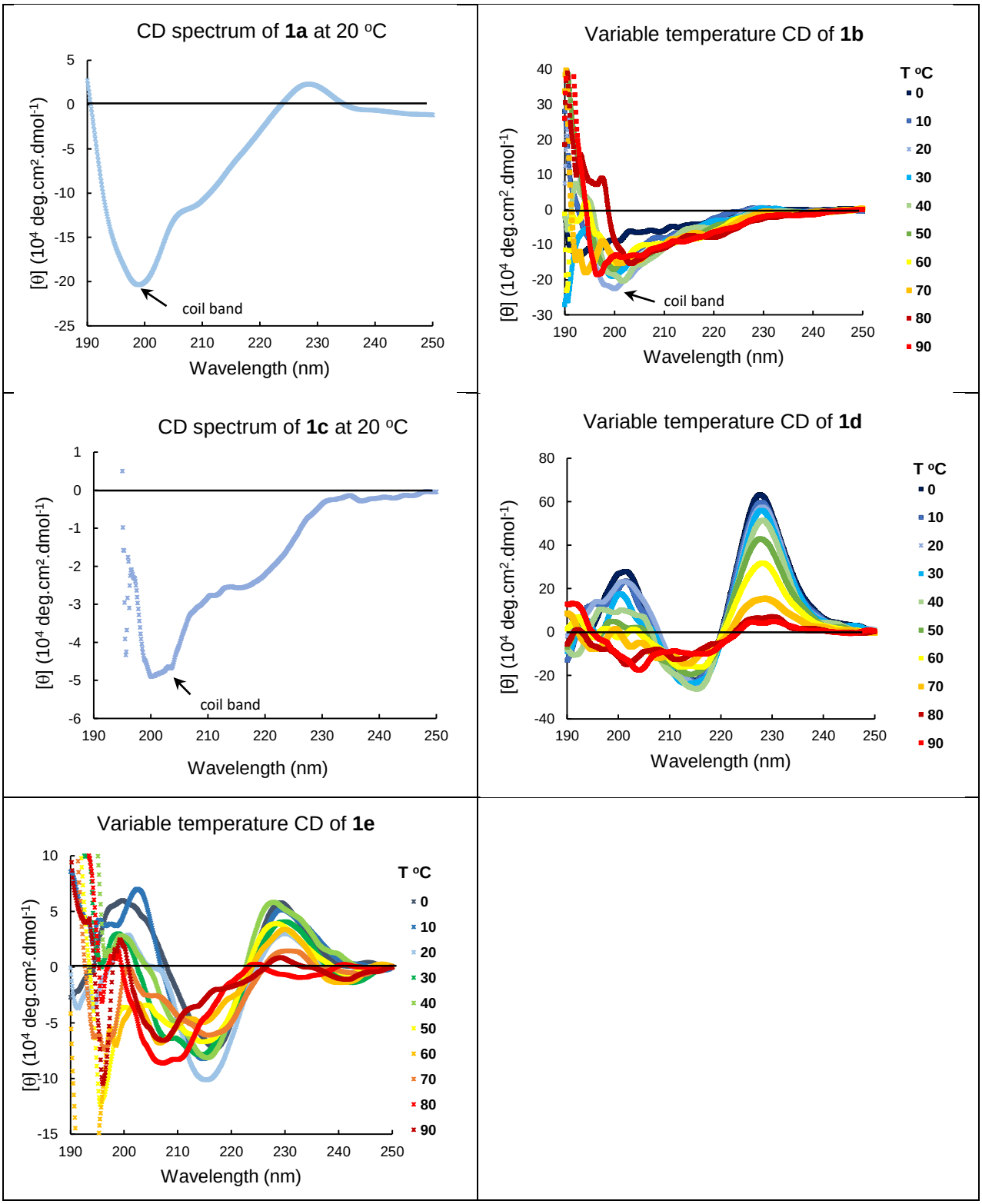

[a] Peptide **1a** was reconstituted in phosphate buffer (15 mM) at C = 24 μM measured by UV-absorbance (Abs_{280} = 0.4307). [b] Peptide **1b** was reconstituted in phosphate buffer (15 mM) at C = 96 μM measured by UV-absorbance (Abs_{280} = 1.651). [c] Peptide **1c** was reconstituted in phosphate buffer (15 mM) / CH_3OH (1:1 v/v) at C = 104 μM measured by UV-absorbance (Abs_{280} = 0.2011). [d] Peptide **1d** was reconstituted in phosphate buffer (15 mM) at C = 30 μM measured by UV-absorbance (Abs_{280} = 0.5879). [e] Peptide **1e** was reconstituted in phosphate buffer (15 mM) / CH_3OH (9:1 v/v) at C = 44 μM measured by UV-absorbance (Abs_{280} = 0.8633).

Figure S10. CD spectra recorded as a function of temperature for peptides **2a-c** [a-c]

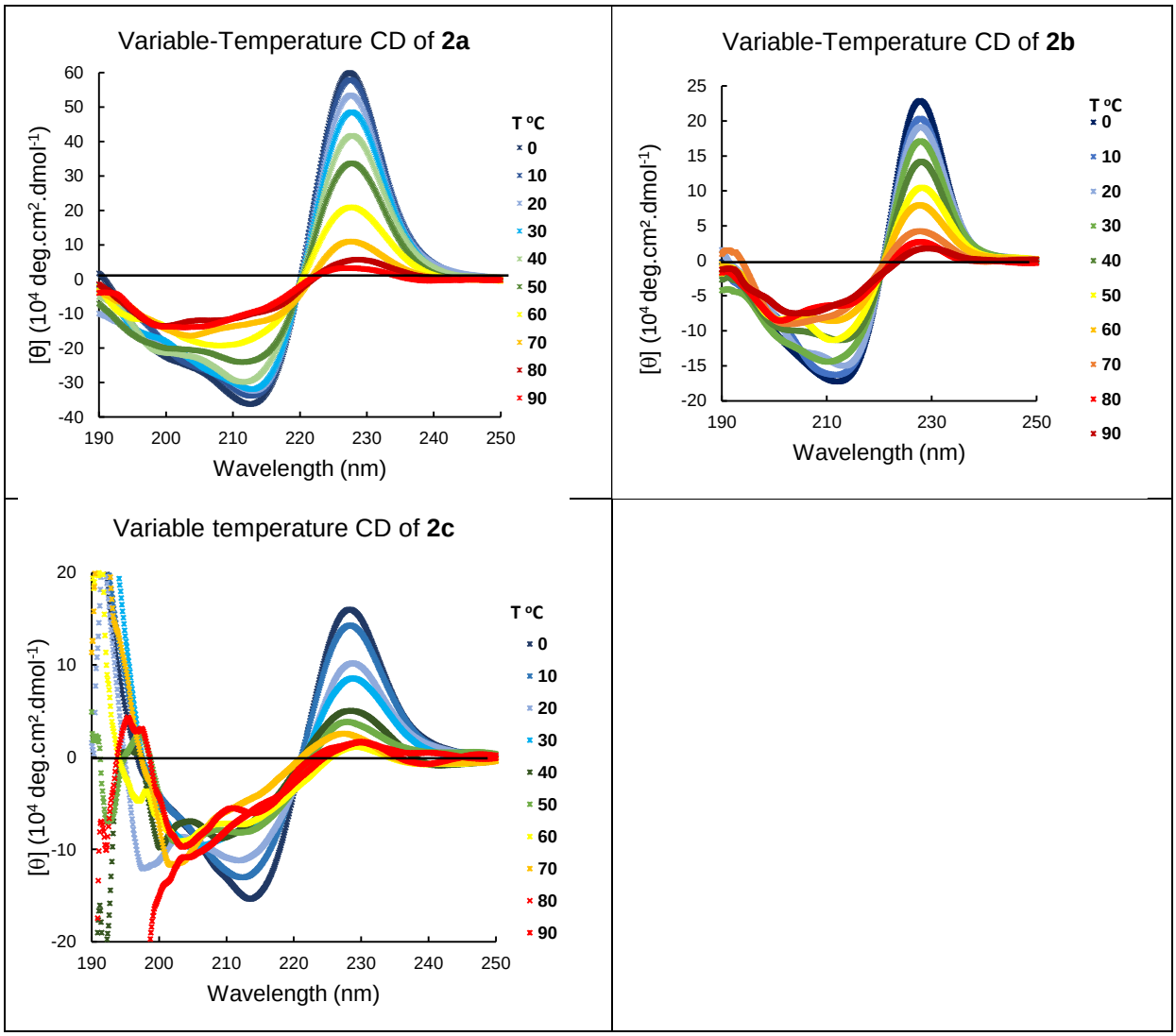

[a] Peptide **2a** was reconstituted in phosphate buffer (15 mM) at C = 38 μM measured by UV-absorbance (Abs_{280} = 0.8575). [b] Peptide **2b** was reconstituted in phosphate buffer (15 mM) at C = 54 μM measured by UV-absorbance (Abs_{280} = 1.2680). [c] Peptide **2c** was reconstituted in phosphate buffer (15 mM) / CH_3OH (9:1 v/v) at C = 35 μM measured by UV-absorbance (Abs_{280} = 0.8333).

Comparative analysis of melting curves (CD) and associated thermodynamic parameters.

Figure S11. Melting curves recorded by variable temperature CD for **1a, 1b, 1d, 1e** and **2a-c**. The folding is represented either by the variation of fraction of folding (right) or molar ellipticity (left) over the temperature.

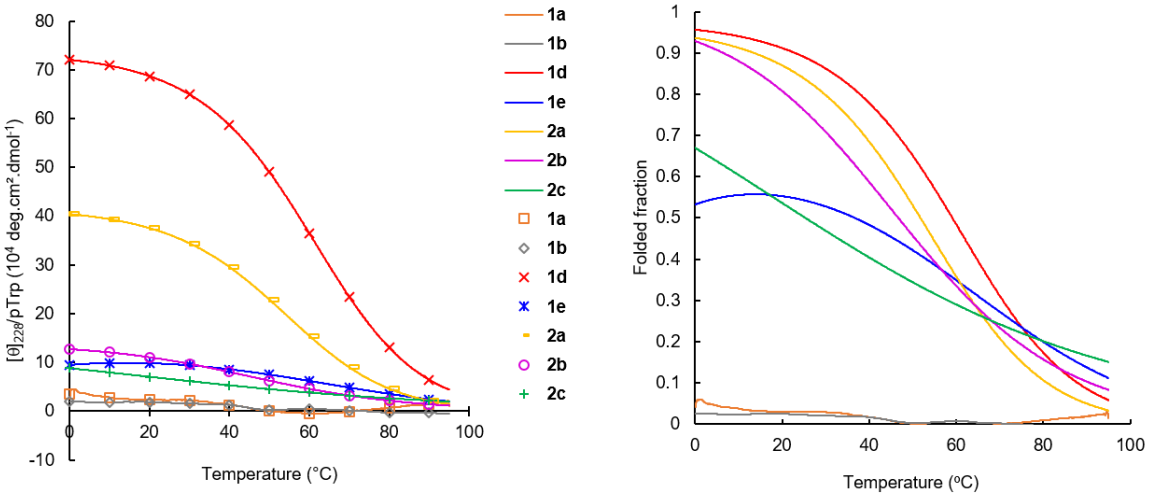

Table S8. Thermodynamic parameters for folded peptides **1d**, **1e** and **2a-c**, calculated from the best-fitted CD melting curves.

Peptide	ΔG_F^o (kcal.mol^{-1})	ΔH_F^o (kcal.mol^{-1})	$T\Delta S_F^o$ (kcal.mol^{-1})	ΔG_F^* (kcal.mol^{-1})	T^* (°C)	T_m (°C)	χ_F (20 °C)
1d	-1.24 ± 0.01	-8.89 ± 0.03	-7.65 ± 0.03	-1.73 ± 0.01	-12 ± 1	59.1 ± 0.1	91 ± 1%
1e	-0.10 ± 0.01	-1.77 ± 0.04	-1.66 ± 0.04	-0.13 ± 0.01	15 ± 1	36.7 ± 0.1	55 ± 1%
2a	-0.98 ± 0.01	-9.27 ± 0.06	-8.29 ± 0.05	-1.54 ± 0.01	-15 ± 1	51.8 ± 0.1	87 ± 1%
2b	-0.69 ± 0.01	-9.67 ± 0.02	-8.97 ± 0.02	-3.18 ± 0.01	-123 ± 1	46.7 ± 0.1	81 ± 1%
2c	-0.01 ± 0.01	-4.77 ± 0.01	-4.76 ± 0.01	-1.51 ± 0.01	-141 ± 1	25.3 ± 0.1	54 ± 1%

b. Structural Characterization by NMR Spectroscopy

Peptides **1a** and **2a-c** were fully characterized previously by our group.[SI6] Peptide **1c** was too poorly soluble in water/DMSO mixtures to be analyzed by NMR. Detailed characterization of **1b, 1d** and **1e** are described below.

Chemical Shift Deviations (CSDs). CSDs were calculated based on a simulated unfolded reference that represents the predicted (calcd.) chemical shift values of a random coil sequence, based on the established work from Poulsen and others.[SI13] The calcd. random coils' chemical shifts for the backbone H_α and H_N protons were obtained from the online software available at: https://spin.niddk.nih.gov/bax/nmrserver/Poulsen_rc_CS/.
The random coil calcd. δ values were validated by comparison to the experimental values obtained for **1a** (Δ|CSD| ≤ 0.20 ppm). CSDs for each hairpin construct were then calculated accordingly to $CSD(H) = \delta H_{exp.} - \delta H_{calcd.}$ and reported in Figure S12. Furthermore, CSD related to the side chains of tryptophan residues have been calculated from the list of known chemical shifts reported on the BMRB database (Biological Magnetic Resonance Bank) for Trp in random coils: http://www.bmrb.wisc.edu/ref_info/pentapeptide.tbl. This list of chemical shifts (Trp random coils) has been previously validated by Andersen *et al*.[SI14]

Figure S12. CSD histograms for peptides **1a, 1d, 1e** and **2a-c**[a] of H_N (Top), H_α (Middle) and tryptophan side chains (Bottom) protons respectively. The $\Delta\delta H\alpha$ Gly from the loop of folded peptides **1d**, **1e** and **2a-c** are also shown in the bottom histogram.

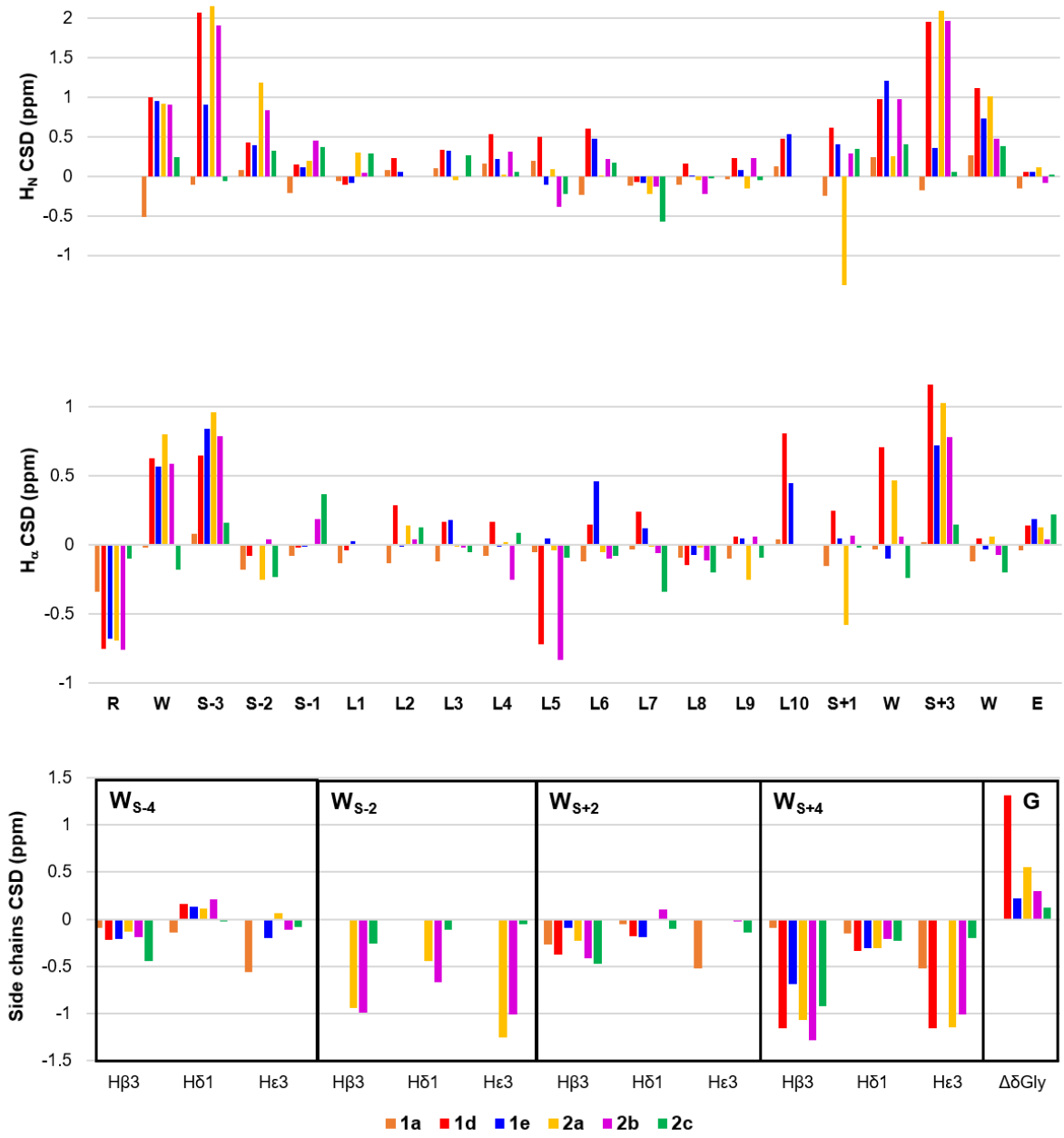

[a] Peptides **1a** and **2a** were prepared in a phosphate buffer (50 mM) /D2O mixture (90:10 v/v) in a 3 to 10 mM concentration range, a 5 mM solution of peptide **1d** was prepared in water/DMSO-d_6 mixture (90:10 v/v), a 3 mM solution of peptide **1e** was prepared in water/DMSO-d_6 mixture (80:20 v/v), a 10 mM solution of peptide **2b** was prepared in water/DMSO-d_6 mixture (85:15 v/v) and a 10 mM solution of peptide **2c** was prepared in a phosphate buffer (50 mM)/DMSO-d_6 mixture (70:30 v/v).

c. Characterization of Novel Peptides by NMR and CD Spectroscopy

Peptide **1b**: RGVAR-RDYRGDPGFD-YWVWE

Figure S13. Thermal Stability of Peptide 1b by CD Spectroscopy. (**A**) Overlay of CD spectra at various temperatures. (**B**) CD Thermal melts plotted from normalized molar elipticity recorded at 228 nm and as fraction of folding (inset).

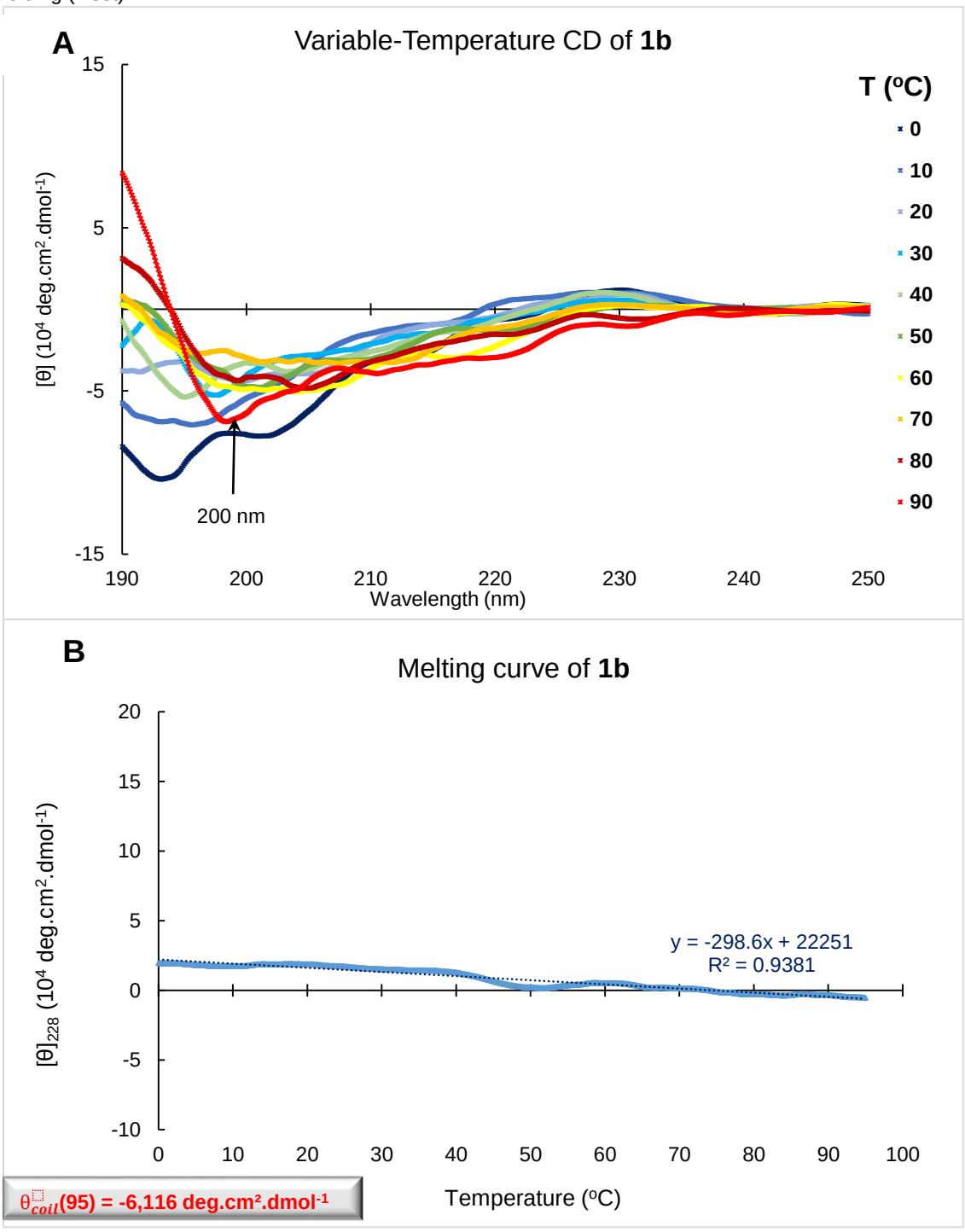

Lyophilized peptide **1b** reconstituted potassium phosphate buffer (pH = 6.5) at C = 96 μM accurately measured by UV-absorbance (Abs_{280} = 1.651).

Figure S14. Thermal Stability of Peptide 1b in a different solvent by CD Spectroscopy. (**A**) Overlay of CD spectra at various temperatures. (**B**) CD Thermal melts plotted from normalized molar elipticity recorded at 228 nm and as fraction of folding (inset).

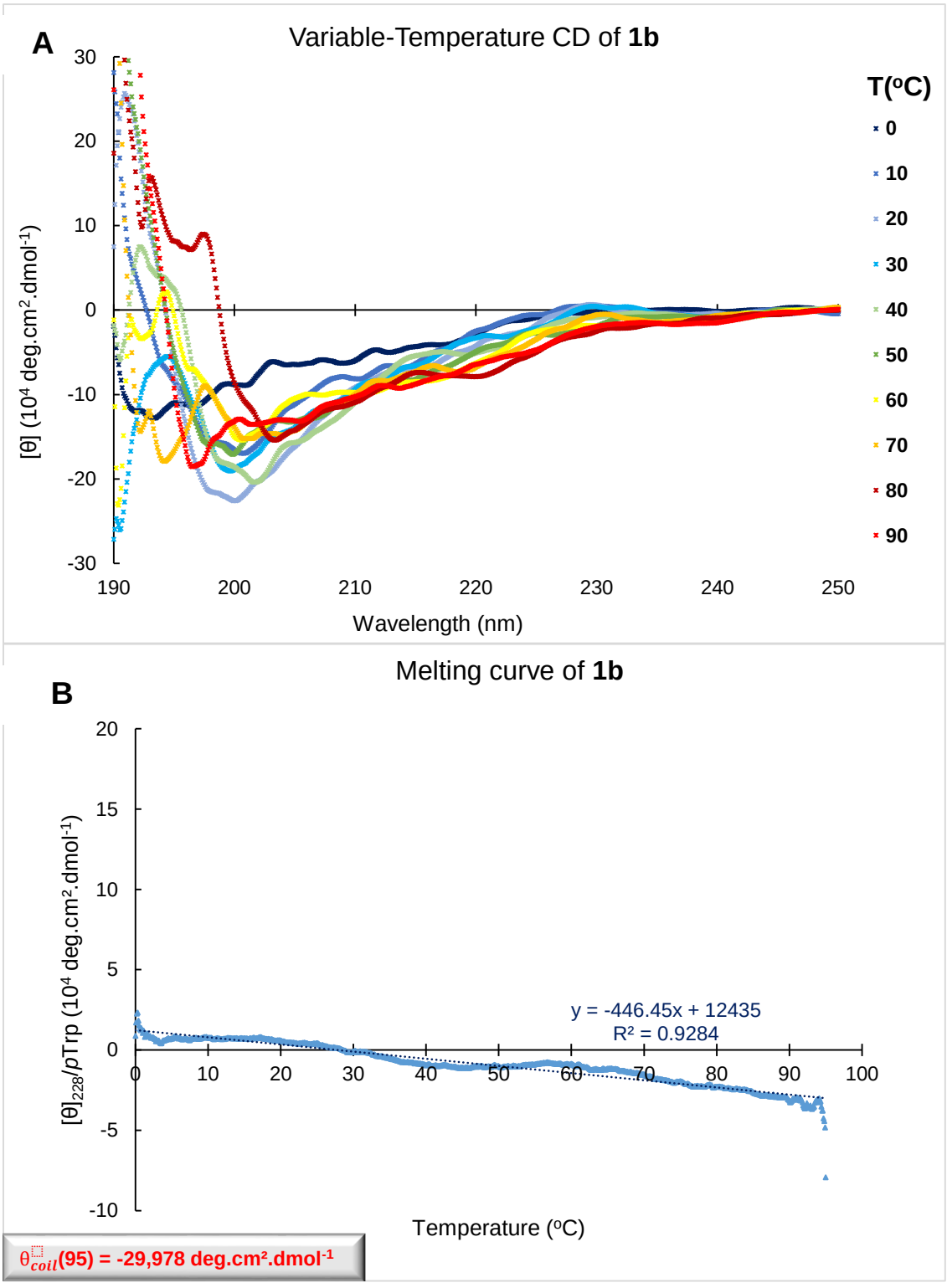

Lyophilized peptide **1b** reconstituted in phosphate buffer (15 mM) / CH_3OH (90:10 v/v) at C = 57 μM accurately measured by UV-absorbance (Abs_{280} = 0.7767).

Peptide **1d**: **RW**VAR-RDYRGDMGFD-YWV**WE**

NMR chemical shift (δ, ppm): Samples were prepared in in water/DMSO-d_6 mixture (90:10 v/v) to improve solubility for the following analysis: ^{1}H, TOCSY, NOESY, ^{1}H-^{13}C HSQC (500 MHz).

Residue (position)	δH^{N}	δH^{α}	δH^{β}	δH other Side chains
R (1)	n.d.	3.51	$H^{\beta2}$: 1.75, $H^{\beta3}$: 1.56	$H^{\gamma2}$: 1.38, $H^{\gamma3}$: 1.30, H^{δ}: 3.08, H^{ε}: 7.21
W (2)	9.10	5.36	$H^{\beta2}$: 3.27, $H^{\beta3}$: 3.12	$H^{\delta1}$: 7.44, $H^{\varepsilon1}$: 10.40, $H^{\zeta2}$: 7.37, $H^{\eta2}$: 7.22, $H^{\zeta3}$: 7.23, $H^{\varepsilon3}$: 7.65
V (3)	9.80	4.56	1.98	$H^{\gamma1}$: 0.85, $H^{\gamma2}$: 0.80
A (4)	8.49	4.08	0.58	
R (5)	8.53	4.31	1.43	H^{γ}: 0.92, $H^{\delta2}$: 3.12, $H^{\delta3}$: 3.06, H^{ε}: 7.17
R (6)	8.30	4.24	$H^{\beta2}$: 1.59, $H^{\beta3}$: 1.53	$H^{\gamma2}$: 1.37, $H^{\gamma3}$: 1.25, H^{δ}: 3.02, H^{ε}: 7.04
D (7)	8.68	4.81	2.62	
Y (8)	8.41	4.70	$H^{\beta2}$: 2.97, $H^{\beta3}$: 2.79	H^{δ}: 6.97, H^{ε}: 6.73
R (9)	8.56	4.40	$H^{\beta2}$: 1.85, $H^{\beta3}$: 1.73	$H^{\gamma2}$: 1.50, $H^{\gamma3}$: 1.42, H^{δ}: 3.11, H^{ε}: 7.18
G (10)	8.66	3.98, 3.76		
D (11)	8.64	4.72	2.96	
M (12)	8.17	4.61	2.11	$H^{\gamma2}$: 2.59, $H^{\gamma3}$: 2.52, H^{ε}: 2.09
G (13)	8.46	**4.13, 3.44**		
F (14)	8.29	4.67	$H^{\beta2}$: 3.08, $H^{\beta3}$: 2.96	H^{δ}: 7.13, H^{ε}: 7.20, H^{ζ}: 7.18
D (15)	8.60	5.24	$H^{\beta2}$: 2.61, $H^{\beta3}$: 2.44	
Y (16)	8.54	4.72	2.99	H^{δ}: 6.86, H^{ε}: 6.53
W (17)	8.61	5.30	$H^{\beta2}$: 3.27, $H^{\beta3}$: 2.96	$H^{\delta1}$: 7.10, $H^{\varepsilon1}$: 10.14, $H^{\zeta2}$: 7.41, $H^{\eta2}$: 7.21, $H^{\zeta3}$: 7.23, $H^{\varepsilon3}$: 7.65
V (18)	9.54	4.98	2.17	$H^{\gamma1}$: 1.04, $H^{\gamma2}$: 0.97
W (19)	8.90	4.59	$H^{\beta2}$: 2.90, $H^{\beta3}$: 2.18	$H^{\delta1}$: 6.94, $H^{\varepsilon1}$: 10.14, $H^{\zeta2}$: 7.41, $H^{\eta2}$: 7.10, $H^{\zeta3}$: 7.04, $H^{\varepsilon3}$: 6.49
E (20)	8.10	4.25	$H^{\beta2}$: 1.94, $H^{\beta3}$: 1.60	H^{γ}: 2.21

Figure S15. Thermal Stability of Peptide 1d by CD Spectroscopy. (**A**) Overlay of CD spectra at various temperatures. (**B**) CD Thermal melts plotted from normalized molar elipticity recorded at 228 nm and as fraction of folding (inset).

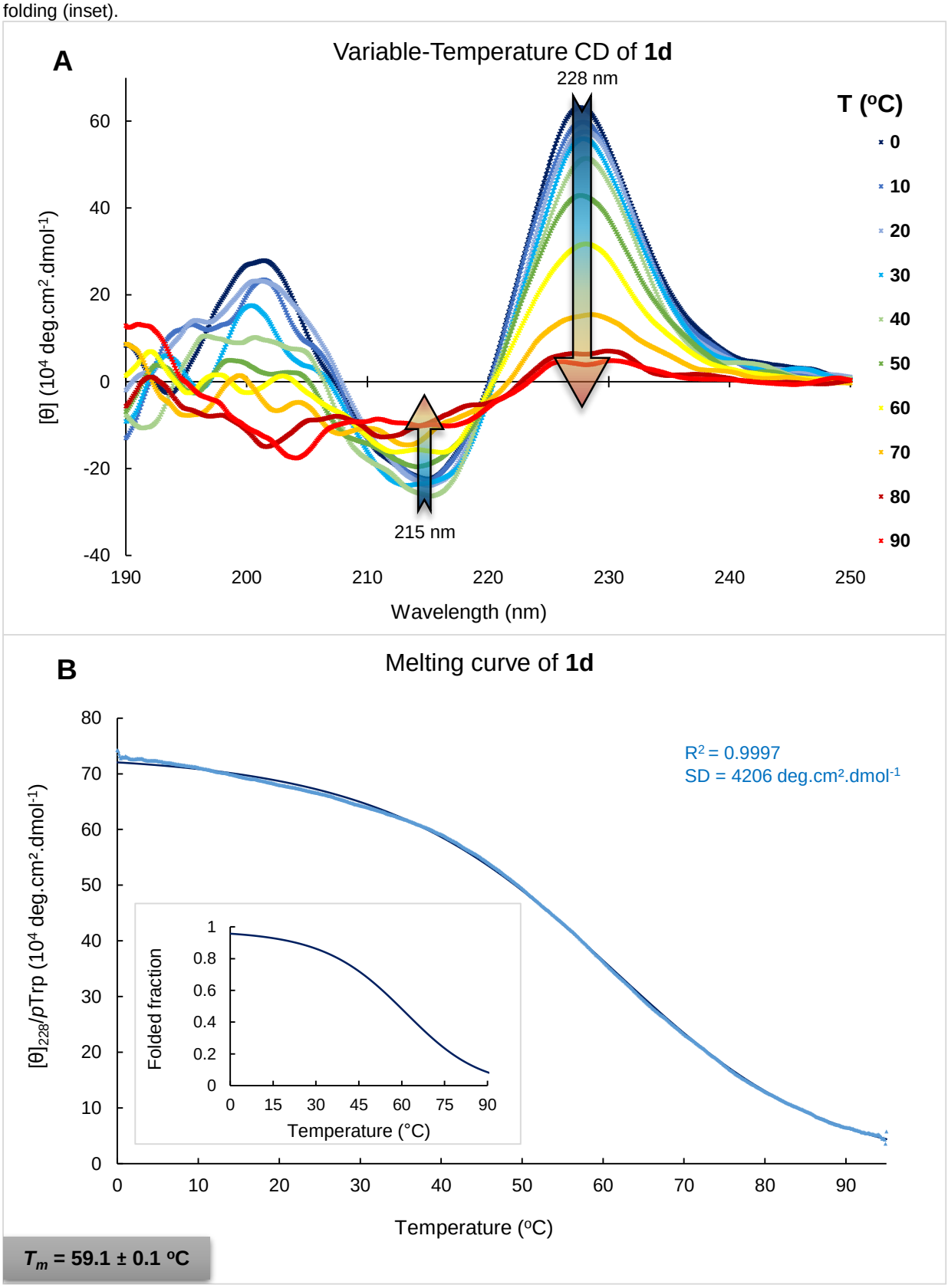

Lyophilized peptide **1d** reconstituted in phosphate buffer (15 mM) at C = 30 μM accurately measured by UV-absorbance (Abs_{280} = 0.5879).

Peptide **1e**: **RW**VAR-RDYRFDMGFD-YWV**WE**

NMR chemical shift (δ, ppm): A 3 mM solution of peptide **1e** was prepared in water/DMSO-d_6 mixture (80:20 v/v) to improve solubility for the following analysis: ^{1}H, TOCSY, NOESY, ^{1}H-^{13}C HSQC (500 MHz).

Residue (position)	δH^N	δH^α	δH^β	δH other Side chains	
R (1)	n.d.	3.58	$H_{\beta2}$: 1.80 $H_{\beta3}$: 1.65	H_γ:1.42, H_δ:3.12, H_ε:7.28	C_β: 28.1, C_γ: 23.2, , C_δ: 40.4
W (2)	9.05	5.30	$H_{\beta2}$:3.28 $H_{\beta3}$:3.13	$H_{\delta1}$:7.41, $H_{\varepsilon1}$:10.43, $H_{\zeta2}$:7.44, $H_{\eta2}$:7.20, $H_{\zeta3}$:7.11, $H_{\varepsilon3}$:7.45	C_β: 27.6, $C_{\delta1}$: 125.2, $C_{\varepsilon3}$: 117.4, $C_{\zeta2}$: 112.6, $C_{\zeta3}$: 121.3, $C_{\eta2}$: 122.3
V (3)	8.64	4.75	2.14	$H_{\gamma1}$: 0.99, $H_{\gamma2}$: 0.94	C_β: 30.7, $C_{\gamma1}$: 18.8, $C_{\gamma2}$: 18.2
A (4)	8.45	4.16	0.72	n.a.	C_β: 19.8
R (5)	8.49	4.32	1.78	H_γ: 1.50, H_δ: 3.12, H_ε: 7.24	C_β: 27.9, C_γ: 24.6, C_δ: 40.4
R (6)	8.32	4.31	$H_{\beta2}$: 1.80 $H_{\beta3}$: 1.61	$H_{\gamma2}$: 1.44, $H_{\gamma3}$: 1.37, H_δ: 3.13, H_ε: 7.25	C_β: 28.4, C_γ: 23.7, C_δ: 40.4
D (7)	8.51	4.51	2.80	n.a.	C_β: 36.8
Y (8)	8.40	4.71	$H_{\beta2}$: 2.99 $H_{\beta3}$: 2.92	H_δ: 6.83, H_ε: 6.58	C_β: 36.9, C_δ: 131.3, C_ε: 115.4
R (9)	8.25	4.22	$H_{\beta2}$: 1.79 $H_{\beta3}$: 1.61	H_γ: 1.36, H_δ: 3.07, H_ε: 7.14	C_β: 28.6, C_γ: 24.1, C_δ: 40.6
F (10)	8.05	4.64	$H_{\beta2}$: 3.15 $H_{\beta3}$: 3.00	H_δ: 7.34, H_ε: 7.22, H_ζ: 7.30	C_β: 40.7, C_δ: 129.0, C_ε: 129.4, C_ζ: 127.4
D (11)	8.52	5.03	$H_{\beta2}$: 2.63 $H_{\beta3}$: 2.52	n.a.	C_β: 36.7
M (12)	8.16	4.49	2.08	H_γ: 2.57, H_δ: 2.16	C_β: 30.7, C_γ: 29.4, C_δ: 14.3
G (13)	8.31	**3.97; 3.75**	n.a.	n.a.	-
F (14)	8.14	4.66	$H_{\beta2}$: 3.11 $H_{\beta3}$: 2.99	H_δ: 7.28, H_ε: 7.17, H_ζ: 7.26	C_β: 40.4, C_δ: 128.9, C_ε: 129.5, C_ζ: 127.4
D (15)	8.65	4.88	$H_{\beta2}$: 2.80 $H_{\beta3}$: 2.68	n.a.	C_β: 38.2
Y (16)	8.32	4.52	$H_{\beta2}$: 3.03 $H_{\beta3}$: 2.86	H_δ: 7.03, H_ε: 6.76	C_β: 36.3, C_δ: 130.7, C_ε: 115.8
W (17)	8.84	4.49	3.25	$H_{\delta1}$: 7.09, $H_{\varepsilon1}$: 10.16, $H_{\zeta2}$: 7.46, $H_{\eta2}$: 7.22, $H_{\zeta3}$: 7.05, $H_{\varepsilon3}$: 7.65	C_β: 27.6, $C_{\delta1}$: 124.4, $C_{\varepsilon3}$: 117.8, $C_{\zeta2}$: 112.6, $C_{\zeta3}$: 119.4, $C_{\eta2}$: 122.5
V (18)	7.94	4.54	2.01	$H_{\gamma1}$: 0.88, $H_{\gamma2}$: 0.82	C_α: n.d., C_β: 30.7, $C_{\gamma1}$: 18.4, $C_{\gamma2}$: 17.8
W (19)	8.51	4.51	$H_{\beta2}$: 3.00 $H_{\beta3}$: 2.65	$H_{\delta1}$: 6.97, $H_{\varepsilon1}$: 10.16, $H_{\zeta2}$: 7.42, $H_{\eta2}$: 7.13, $H_{\zeta3}$: 7.13, $H_{\varepsilon3}$: 7.65	C_β: 24.0, $C_{\delta1}$: 125.8, $C_{\varepsilon3}$: 117.9, $C_{\zeta2}$: 112.6, $C_{\zeta3}$: 119.4, $C_{\eta2}$: 122.5
E (20)	8.10	4.30	$H_{\beta2}$: 1.99 $H_{\beta3}$: 1.66	H_γ: 2.25	C_β: 27.0, C_γ: 30.1

Figure S16. Thermal Stability of Peptide 1b by CD Spectroscopy. (**A**) Overlay of CD spectra at various temperatures. (**B**) CD Thermal melts plotted from normalized molar elipticity recorded at 229 nm and as fraction of folding (inset).

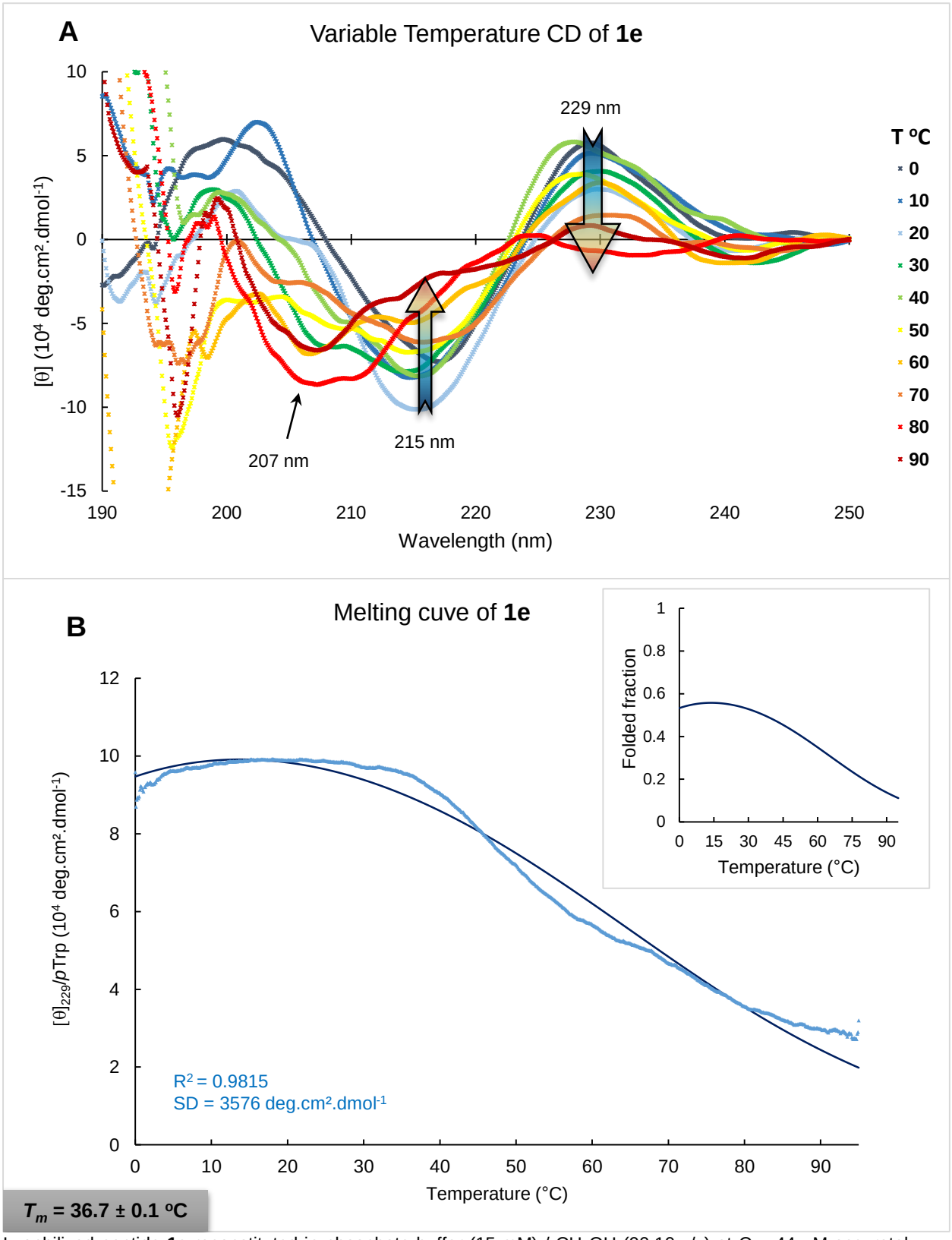

Lyophilized peptide **1e** reconstituted in phosphate buffer (15 mM) / CH_3OH (90:10 v/v) at C = 44 μM accurately measured by UV-absorbance (Abs_{280} = 0.8633).

7. PD1/PDL1 ImmunoBlocking Assay Results

Figure S17. Dose response curves from the ELISA binding assay showing inhibition of the PD1/PDL1 interaction with various inhibitors. **A.** Control experiments with pembrolizumab and other commercially available PD-L1 inhibitors. **B.** Peptide inhibitors mimics of the pembrolizumab H3 loop and the unfolded analog **1b** as negative control.

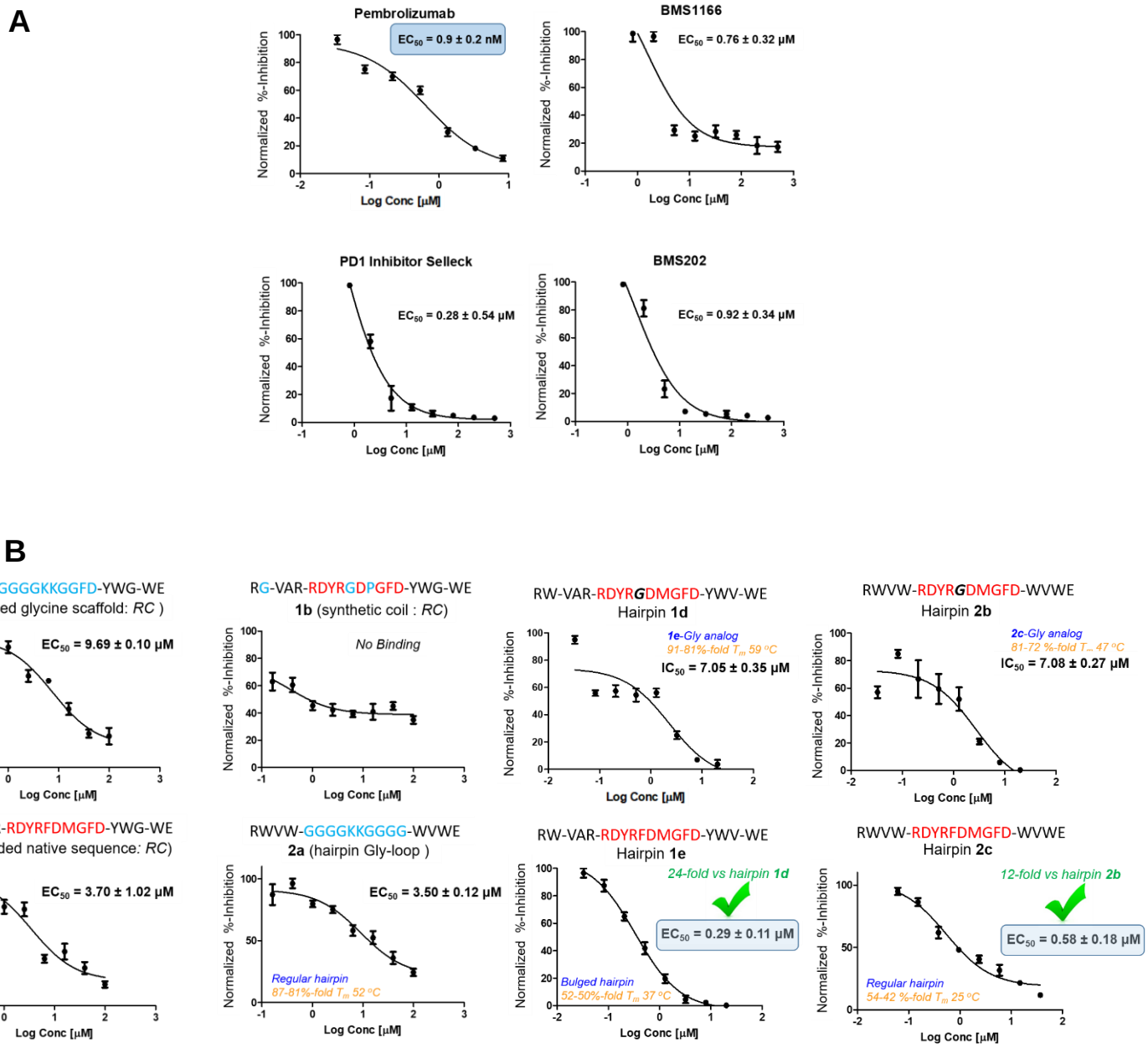

8. Competitive Binding Kinetics

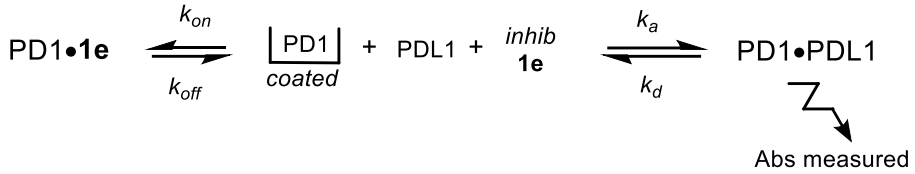

A UV-Vis assay was developed to determine the competitive binding of PD1 to hairpin **1e** and PDL1. Model kinetic curves for a competitive PDL1 inhibition assay with inhibitor **1e** were generated accordingly to a reported procedure by S. R. J. Horae.[SI15] Raw absorbance readouts of the [PD1•PDL1] complex formation were measured every 10 minutes and corrected by subtracting non-specific binding absorbance values (data points obtained from a quasi-irreversible binding at high concentration >3.0 μM). The corrected raw absorbance of the [PD1•PDL1] complex tracer ($A_{PDL1/PD1}$) were plotted as a function of time (t) and fitted with a nonlinear least square fitting routine in OriginPro 9.0, to the following equation:

Eq. S8

$$A_{PDL1/PD1} = \frac{A_{max}[PDL1]k_a}{K_F-K_S}\left[\frac{k_{off}(K_F-K_S)}{K_FK_S} + \frac{k_{off}-K_F}{K_F}e^{-K_Ft} - \frac{k_{off}-K_S}{K_S}e^{-K_St}\right] - \frac{A_{max}[PDL1]k_a[\mathbf{1e}]k_{on}}{(K_F-K_S)([\mathbf{1e}]k_{on}+k_{off})}\left(1-e^{-([\mathbf{1e}]k_{on}+k_{off})t_P}\right)(e^{-K_St}-e^{-K_Ft})$$

with

$$K_F = 0.5\left([PDL1]k_a + k_d + [\mathbf{1e}]k_{on} + k_{off} + \sqrt{\left([PDL1]k_a + k_d - [\mathbf{1e}]k_{on} - k_{off}\right)^2 + 4[PDL1][\mathbf{1e}]k_ak_{on}}\right)$$ Eq. S9

$$K_S = 0.5\left([PDL1]k_a + k_d + [\mathbf{1e}]k_{on} + k_{off} - \sqrt{\left([PDL1]k_a + k_d - [\mathbf{1e}]k_{on} - k_{off}\right)^2 + 4[PDL1][\mathbf{1e}]k_ak_{on}}\right)$$ Eq. S10

and k_a, k_d, being the association and dissociation rate constants of PDL1 respectively, k_{on}, k_{off}, being the association and dissociation rate constants of **1e** respectively, A_{max} the maximum absorbance measured at equilibrium (plateau for **1e** at 375 nM), and t_p the pre-incubation time.

Fitting Protocol. Sets of raw data at each concentration of **1e** (0.375, 0.75, and 1.50 μM) were fitted separately. For the nonlinear least-square fitting routine, k_a and k_d values reported by Kim and coworkers (36,000 $M^{-1}.s^{-1}$, 0.15 s^{-1} respectively)[SI16], as well as the initial concentrations of PDL1 (560 μM), [**1e**], t_p (3600 s), and A_{max} value of 1.0 were imputed in OriginPro 9.0, while k_{on} and k_{off} were allowed to vary to generate the best-fitted kinetic curves corresponding to Eq. S8. The fitting procedure was initiated using arbitrary values for k_{on} and k_{off} of 98000 $M^{-1}.s^{-1}$ and 0.00001 s^{-1} respectively and the results presented in Table S9. The computed best-fitted curves were exploited to calculate K_i values based on the following equation:

$$K_i = \frac{k_{off}}{k_{on}}$$ Eq. S11

Table S9. Parameters imputed and computed from the nonlinear least-square fitting routine for hairpin **1e** in a PDL1 competitive binding inhibition assay.

[**1e**] (nM)	A_{max} (a.u.) [a]	k_{on} (10^4 $M^{-1}.s^{-1}$) [b]	k_{off} (10^{-4} s^{-1}) [b]	K_i (nM)	RMSD (a.u.)
375	1.0	1.05 ± 0.81	6.23 ± 0.96	58.9 ± 36.2	0.031
750	1.0	1.67 ± 0.94	4.55 ± 0.75	27.2 ± 11.4	0.058
1500	1.0	0.56 ± 0.67	2.15 ± 0.51	38.2 ± 36.7	0.052
Avg.[c]	-	**1.10 ± 0.81**	**4.31 ± 0.74**	**41.4 ± 28.1**	**0.047**

[a] Maximum absorbance corresponding to the maximum PD1/PDL1 complex formation at the binding equilibrium (kinetic plateau). [b] k_{on}, k_{off}, K_i and their respective standard error generated by the kinetic fitting protocol. [c] k_{on}, k_{off} and K_i Values were averaged from the three best-fitted kinetic curves.

Selected 1D- and 2D-NMR Spectra

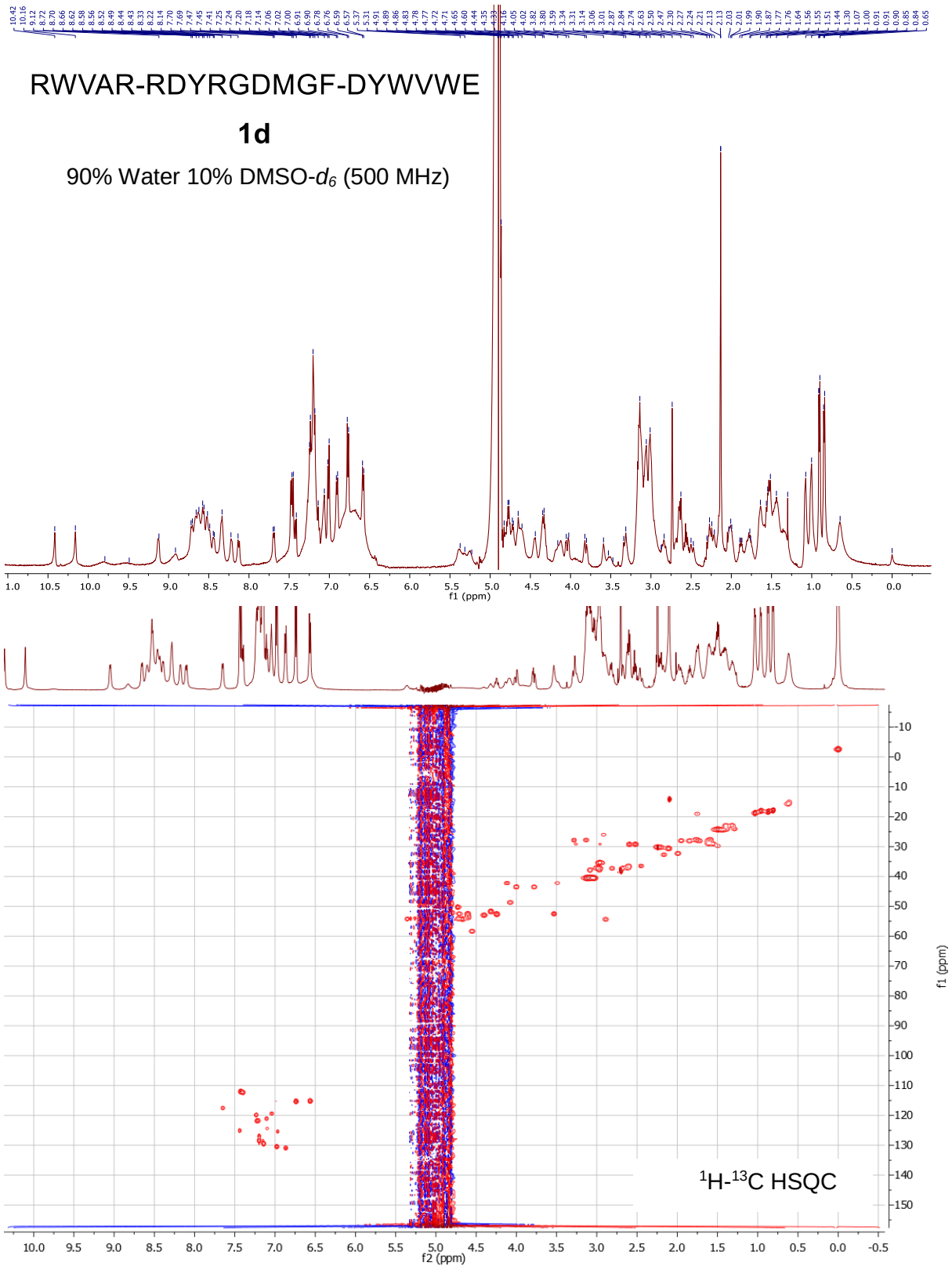

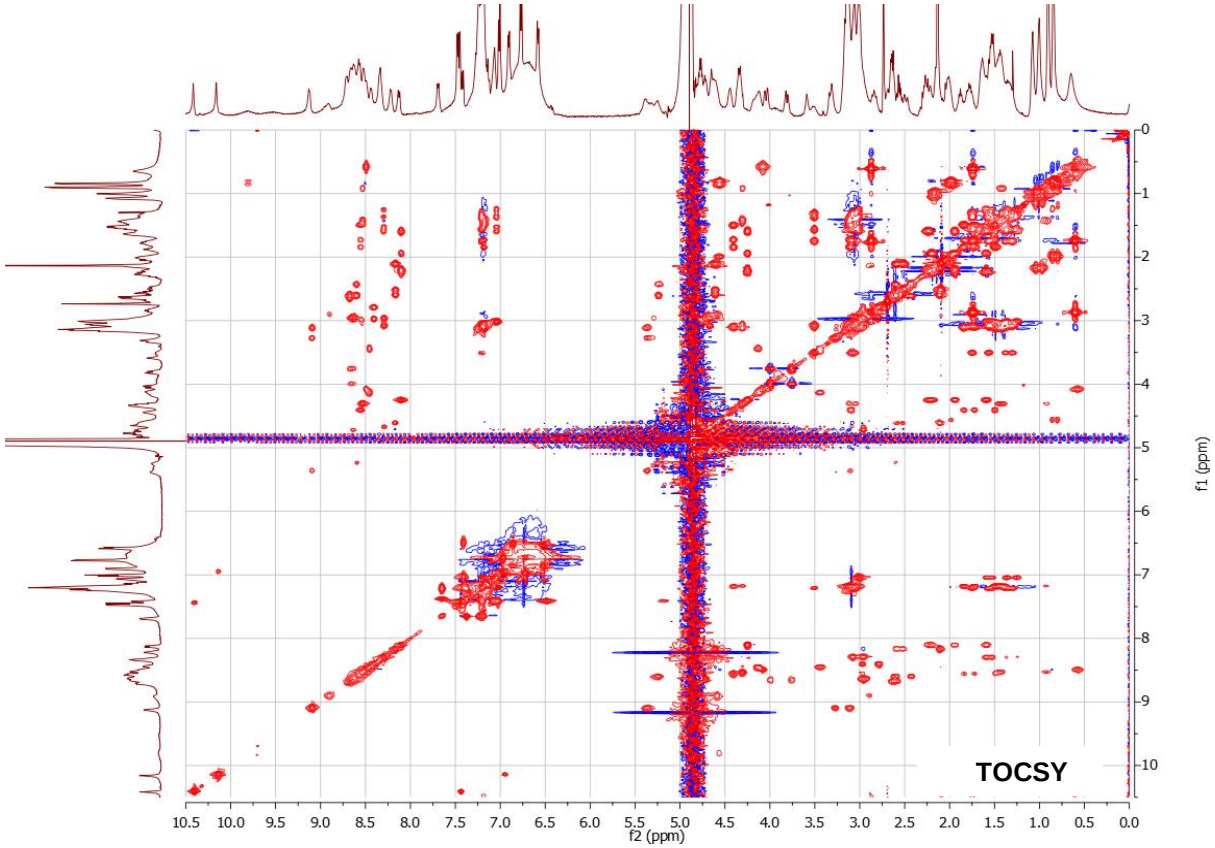
TOCSY
f2 (ppm)
f1 (ppm)

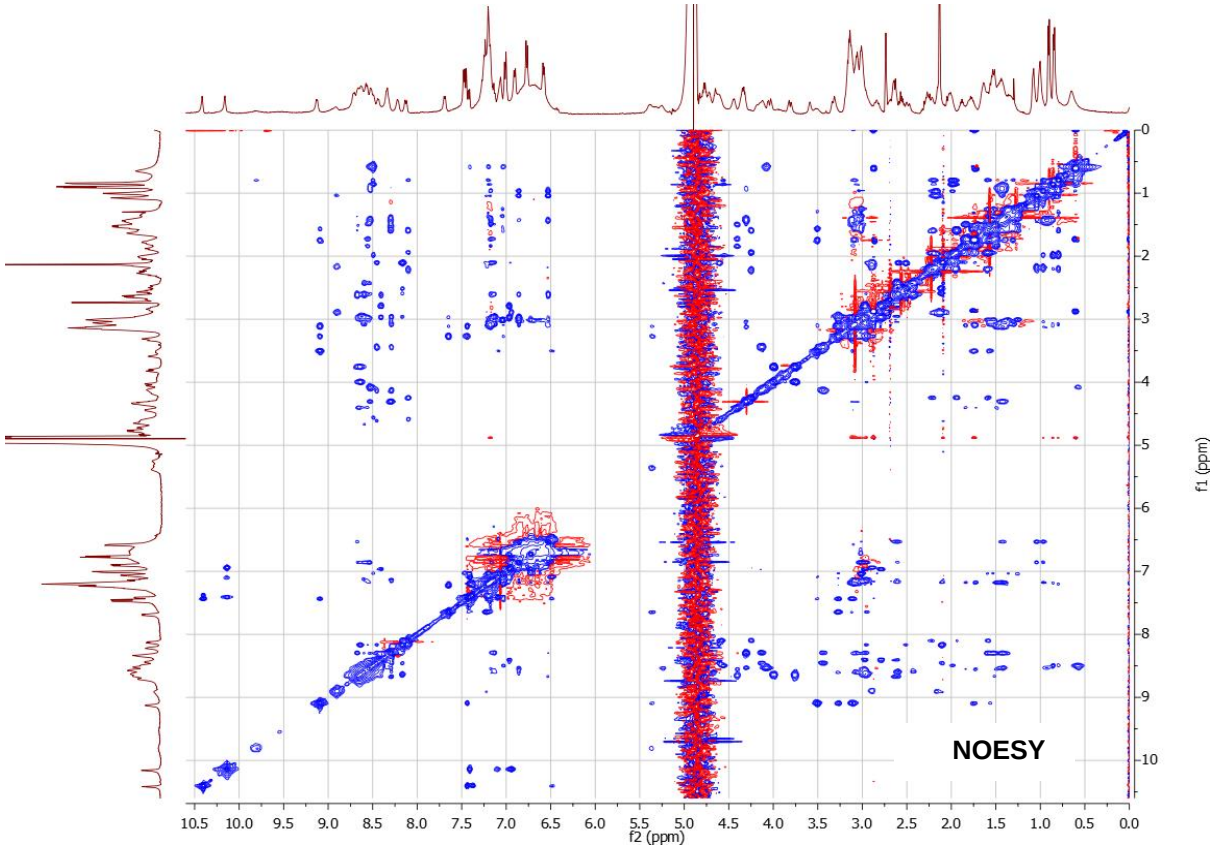
NOESY
f2 (ppm)
f1 (ppm)

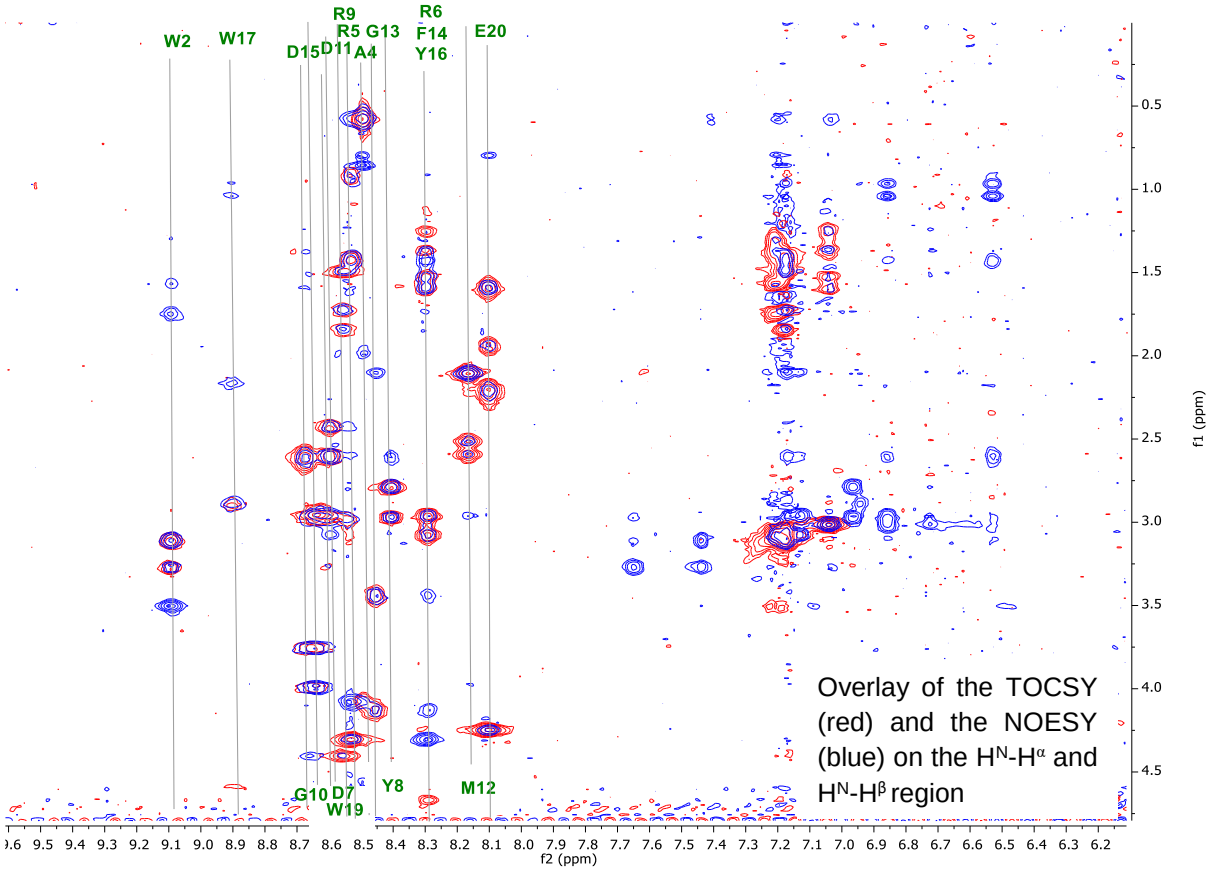
W2
W17
D15
R9
R5
D11
G13
A4
R6
F14
Y16
E20
G10
D7
W19
Y8
M12
f2 (ppm)
f1 (ppm)
Overlay of the TOCSY (red) and the NOESY (blue) on the H^N-H^α and H^N-H^β region

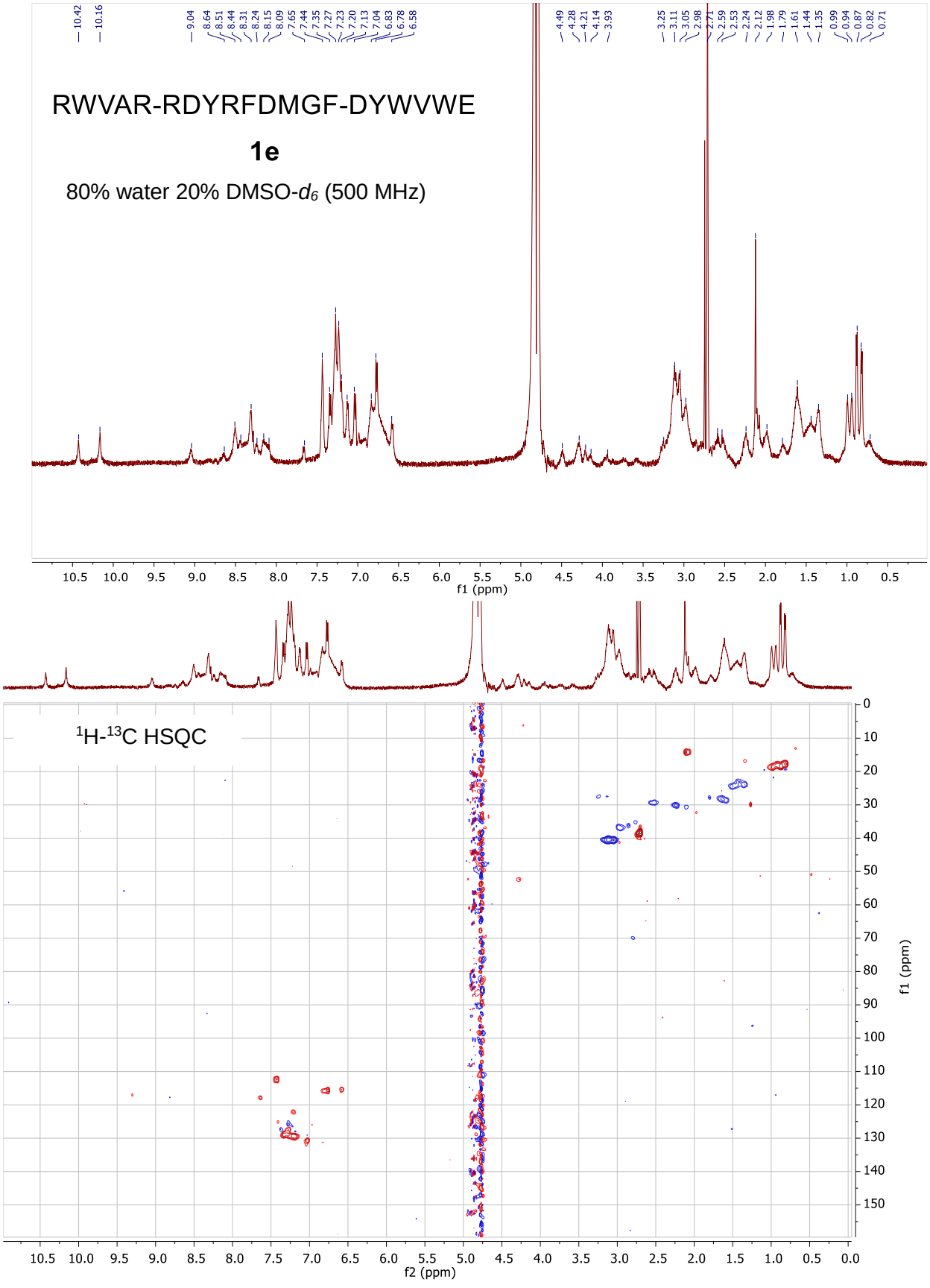
RWVAR-RDYRFDMGF-DYWVWE
1e
80% water 20% DMSO-d_6 (500 MHz)
10.42
10.16
9.04
8.64
8.51
8.44
8.31
8.24
8.15
8.09
7.65
7.44
7.35
7.27
7.23
7.20
7.13
7.04
6.83
6.78
6.58
4.49
4.28
4.21
4.14
3.93
3.25
3.11
3.05
2.98
2.71
2.59
2.53
2.24
2.12
1.98
1.79
1.61
1.44
1.35
0.99
0.94
0.87
0.82
0.71
f1 (ppm)
^{1}H-^{13}C HSQC
f2 (ppm)
f1 (ppm)

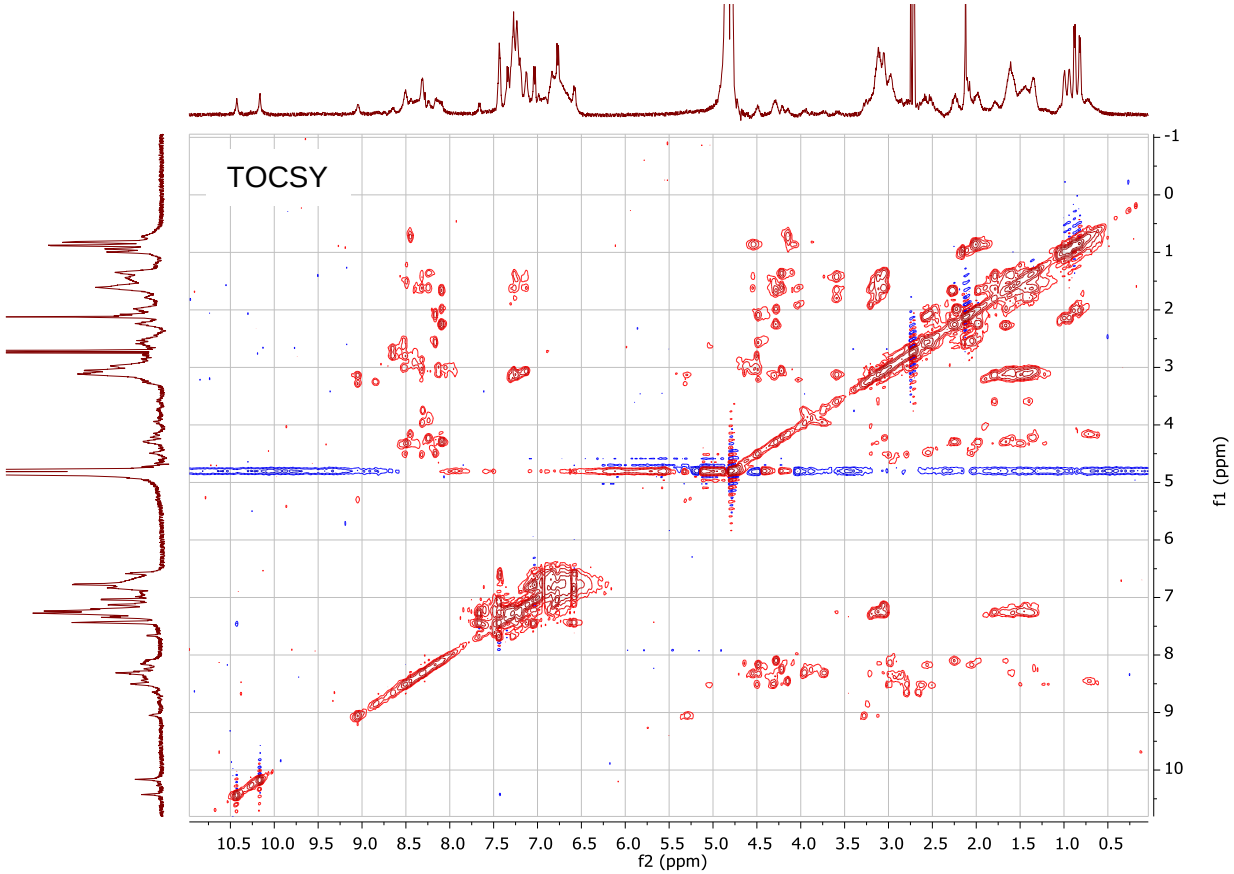
TOCSY
f2 (ppm)
f1 (ppm)

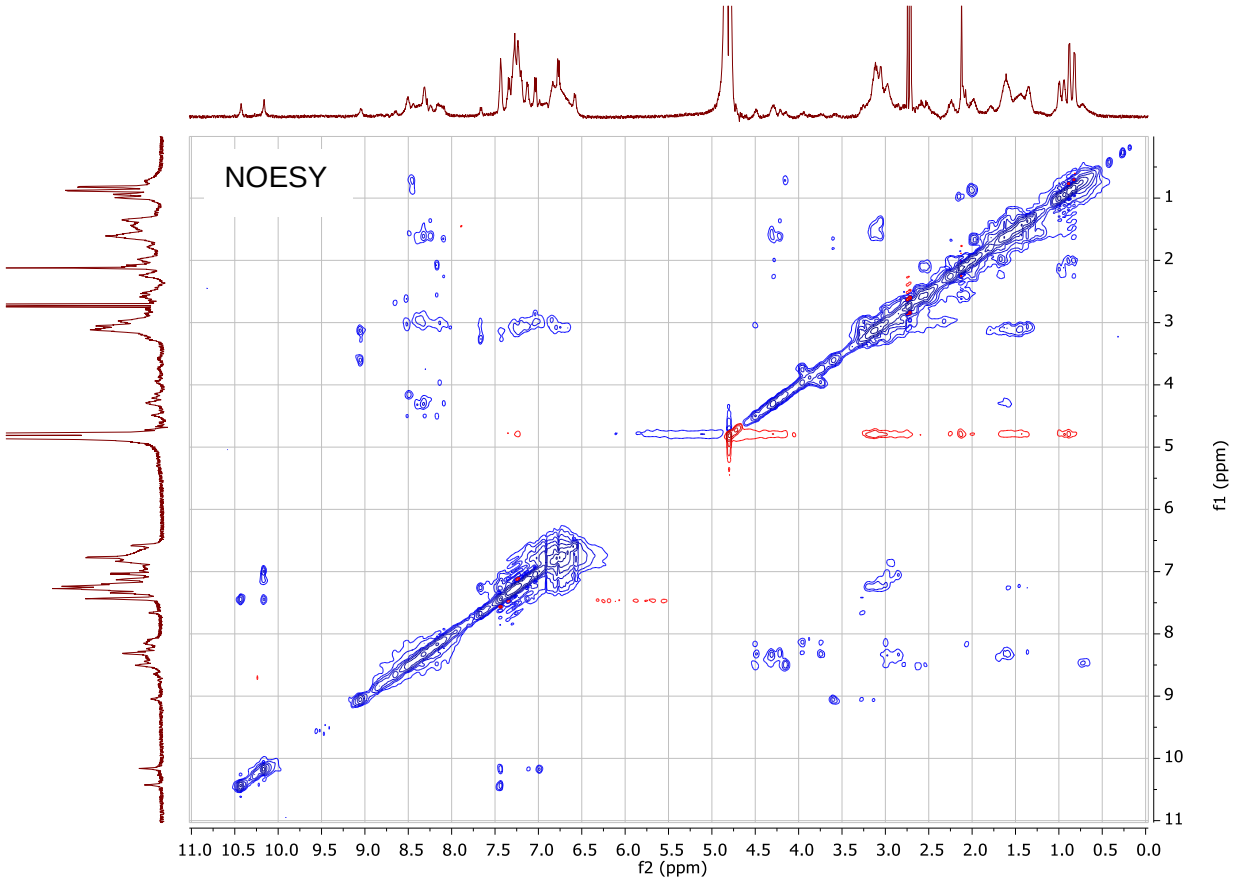
NOESY
f2 (ppm)
f1 (ppm)

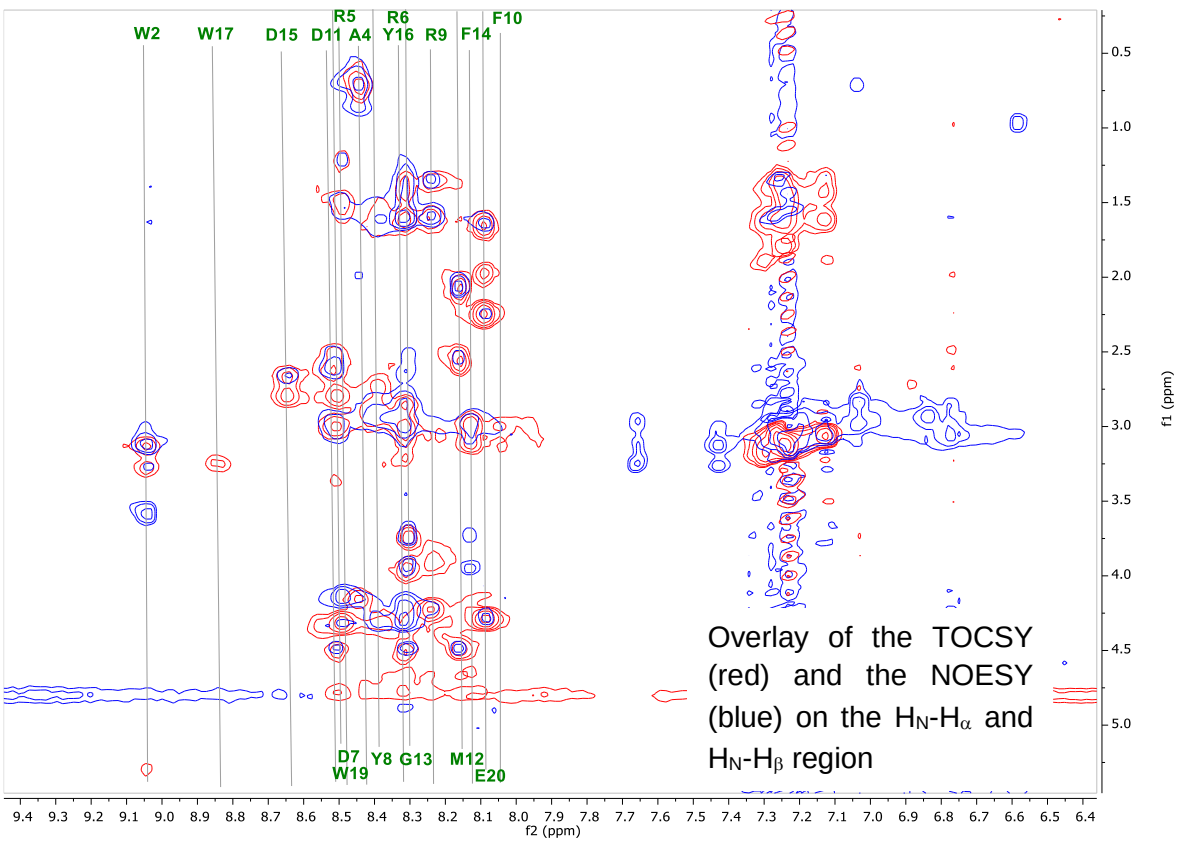
W2
W17
D15
R5
D11
A4
R6
Y16
R9
F14
F10
D7
W19
Y8
G13
M12
E20
f2 (ppm)
f1 (ppm)
Overlay of the TOCSY (red) and the NOESY (blue) on the H_N-H_α and H_N-H_β region

RWVW-GGGGKKGGGG-WVWE

2a

90% buffer 10% D_2O (500 MHz)

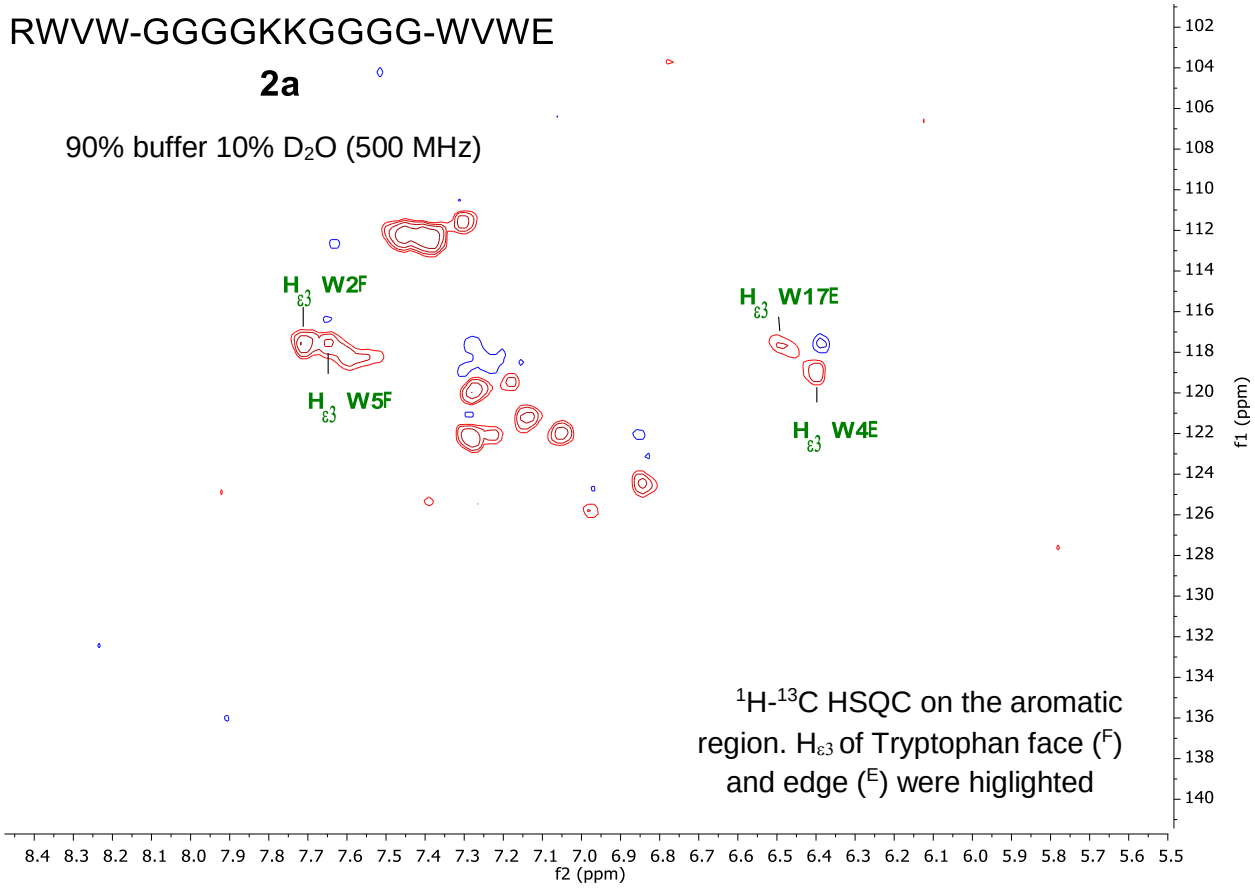

^{1}H-^{13}C HSQC on the aromatic region. $H_{\varepsilon 3}$ of Tryptophan face (^{F}) and edge (^{E}) were higlighted

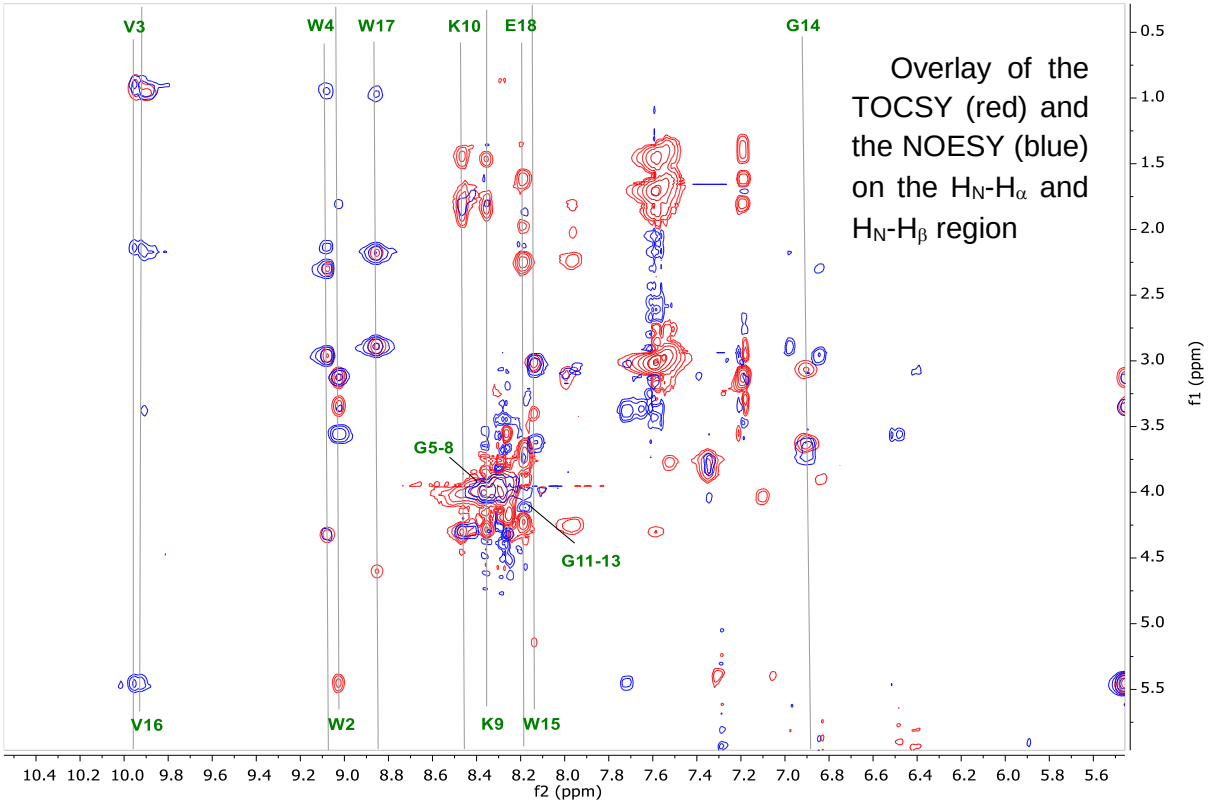

Overlay of the TOCSY (red) and the NOESY (blue) on the H_N-H_α and H_N-H_β region

References

[SI1] Laskowski, R. A.; Swindells, M. B. LigPlot+: Multiple Ligand–Protein Interaction Diagrams for Drug Discovery. *J. Chem. Inf. Model.* **2011**, *51*, 2778.

[SI2] The PyMOL Molecular Graphics System, Version 2.0 Schrödinger, LLC

[SI3] (a) Pettersen, E. F.; Goddard, T. D.; Huang, C. C.; Couch, G. S.; Greenblatt, D. M.; Meng, E. C.; Ferrin, T. E. UCSF Chimera—A Visualization System for Exploratory Research and Analysis. *J. Comput. Chem.* **2004**, *25*, 1605. (b) Webb, B.; Sali, A. Comparative Protein Structure Modeling Using MODELLER. *Curr. Protoc. Bioinformatics* **2016**, *54*, 5.6.1-5.6.37.

[SI4] (a) Chaudhury, S.; Lyskov, S.; Gray, J. J. PyRosetta: A Script-Based Interface for Implementing Molecular Modeling Algorithms Using Rosetta. *Bioinformatics* **2010**, *26*, 689–691. (b) Schenkelberg, C. D.; Bystroff, C. InteractiveROSETTA: A Graphical User Interface for the PyRosetta Protein Modeling Suite. *Bioinformatics* **2015**, *31*, 4023.

[SI5] Gu, Y.; Li, D.-W.; Brüschweiler, R. Statistical Database Analysis of the Role of Loop Dynamics for Protein–Protein Complex Formation and Allostery. *Bioinformatics* **2017**, *33*, 1814.

[SI6] Richaud, A. D.; Zhao, G.; Hobloss, S.; Roche, S. P. Folding in Place: Design of β-Strap Motifs to Stabilize the Folding of Hairpins with Long Loops. *J. Org. Chem.* **2021**, *86*, 13535.

[SI7] Na, Z.; Yeo, S. P.; Bharath, S. R.; Bowler, M. W.; Balıkçı, E.; Wang, C.-I.; Song, H. Structural Basis for Blocking PD-1-Mediated Immune Suppression by Therapeutic Antibody Pembrolizumab. *Cell Res.* **2017**, *27*, 147.

[SI8] Horita, S.; Nomura, Y.; Sato, Y.; Shimamura, T.; Iwata, S.; Nomura, N. High-Resolution Crystal Structure of the Therapeutic Antibody Pembrolizumab Bound to the Human PD-1. *Sci. Rep.* **2016**, *6*, 35297.

[SI9] Lee, J. Y.; Lee, H. T.; Shin, W.; Chae, J.; Choi, J.; Kim, S. H.; Lim, H.; Won Heo, T.; Park, K. Y.; Lee, Y. J.; et al. Structural Basis of Checkpoint Blockade by Monoclonal Antibodies in Cancer Immunotherapy. *Nat. Commun.* **2016**, *7*, 13354.

[SI10] Ribeiro, J.; Ríos-Vera, C.; Melo, F.; Schüller, A. Calculation of Accurate Interatomic Contact Surface Areas for the Quantitative Analysis of Non-Bonded Molecular Interactions. *Bioinformatics* **2019**, *35*, 3499.

[SI11] Greenfield, N. J. Using Circular Dichroism Collected as a Function of Temperature to Determine the Thermodynamics of Protein Unfolding and Binding Interactions. *Nat. Protoc.* **2006**, *1*, 2527.

[SI12] Becktel, W. J.; Schellman, J. A. Protein Stability Curves. *Biopolymers* **1987**, *26*, 1859.

[SI13] (a) Schwarzinger, S.; Kroon, G.J.; Foss, T.R.; Chung. J.; Wright, P.E.; Dyson, H. J. Sequence-dependent correction of random coil NMR chemical shifts. *J. Am. Chem. Soc.* **2001**, *123,* 2970. (b) Kjaergaard, M.; Poulsen, F.M. Sequence correction of random coil chemical shifts: correlation between neighbor correction factors and changes in the Ramachandran distribution. *J. Biomol. NMR* **2011**, *50*, 157. (c) Kjaergaard, M.; Brander, S.; Poulsen, F.M. Random coil chemical shifts for intrinsically disordered proteins: Effects of temperature and pH. *J. Biomol. NMR,* **2011**, *49*,139.

[SI14] Andersen, N. H.; Olsen, K. A.; Fesinmeyer, R. M.; Tan, X.; Hudson, F. M.; Eidenschink, L. A.; Farazi, S. R. Minimization and Optimization of Designed β-Hairpin Folds. *J. Am. Chem. Soc.* **2006**, *128*, 6101.

[SI15] Hoare, S. R. J. Analyzing Kinetic Binding Data. In *Assay Guidance Manual [Internet]* Markossian, S., Grossman, A., Brimacombe, K., Eds.; Bethesda (MD): Eli Lilly & Company and the National Center for Advancing Translational Sciences, **2021**.

[SI16] Tang, S.; Kim, P. S. A high-affinity human PD-1/PD-L2 complex informs avenues for small-molecule immune checkpoint drug discovery. *Proc. Natl. Acad. Sci. USA* **2019**, *116*, 24500.